J. Fluid Mech. (1989), *vol.* 204, *pp.* 325–358
Printed in Great Britain

Modal exchange mechanisms in Lapwood convection

By D. S. RILEY[1] AND K. H. WINTERS[2]

[1] School of Mathematics, University of Bristol, Bristol BS8 1TW, UK
[2] Theoretical Physics Division, Harwell Laboratory, Didcot, Oxon OX11 0RA, UK

(Received 9 June 1988)

Techniques of bifurcation theory are used to study the porous-medium analogue of the classical Rayleigh–Bénard problem: Lapwood convection in a two-dimensional saturated porous cavity heated from below. Two particular aspects of the problem are focused upon: (i) the existence of multiple steady solutions and (ii) the influence of aspect ratio.

Convection begins only when the applied temperature difference (say) exceeds a critical value defined by linear stability theory. The resulting convective flow pattern depends both on the magnitude of the temperature difference and on the aspect ratio of the cavity. A weakly nonlinear analysis reveals the roles played by so-called secondary bifurcations in determining the formation of further, anomalous patterns at fixed aspect ratio. In addition to giving rise to alternative stable flows for identical operating conditions, the secondary bifurcations are required for the modal exchanges which take place as the aspect ratio varies, a process which causes an abrupt change in preferred flow pattern at certain critical values of the aspect ratio.

As a complement to and an extension of the weakly nonlinear analysis, numerical methods are used to determine the bifurcation processes and to elucidate the modal exchange mechanisms in both weakly and strongly convective flows. The effect of container size is studied by continuation methods to predict the variation of the critical Rayleigh number of the bifurcation points for aspect ratios in the range 0.5 to 2.0. In this way a stability map is obtained which shows the alternative patterns expected for particular operating conditions. The Nusselt number is computed and it is found that the alternative stable modes transfer significantly different amounts of heat through the medium.

The study has provided new information on the existence and characteristics of, and interactions between, alternative steady modes of two-dimensional Lapwood convection. The results have important ramifications for the modelling and design of physical systems in which convective flow in a saturated porous medium is stimulated by an imposed unstable temperature gradient.

1. Introduction

Convective flows in porous media are of interest in many varied practical situations: in geothermal energy resource and oil-reservoir modelling, in mass transfer through snow layers and the genesis of avalanches, in open-pore insulation systems and in gas flows through tobacco rods, to name but a few. These sorts of applications, together with the fact that the study of porous-media flows is a fundamental scientific problem, have motivated a rapidly increasing number of

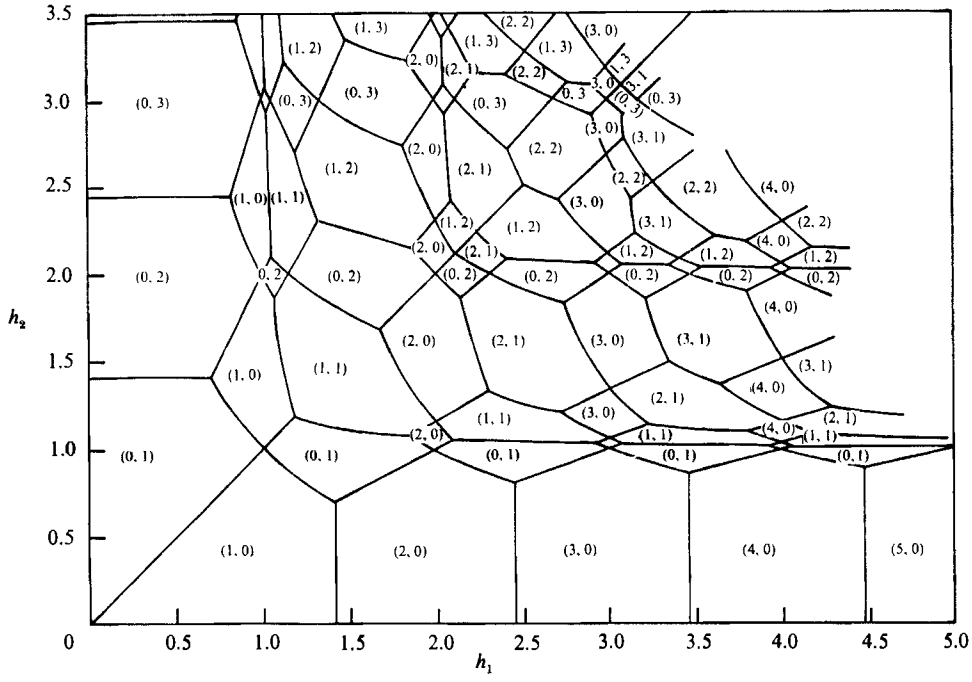

FIGURE 1. Map showing how the horizontal wavevector (m, n) of the most linearly unstable disturbance depends on the aspect ratios h_1, h_2 of an untilted rectangular cell. The vertical wavenumber for these modes is unity. (After Beck 1972.)

investigations in the last decade. A recent survey of the literature on free-convective flows in porous media may be found in the excellent review by Bories (1985).

The present study is concerned with the bifurcation structure associated with steady free convection in a finite two-dimensional saturated porous cavity heated from below. The aim of this study is to identify stable regimes and to describe the interchange processes which take place when the aspect ratio varies.

Beck (1972) seems to have been the first to consider convection in a finite three-dimensional horizontal box of porous material saturated with fluid and heated from below. Using linear stability analysis, he found the critical Rayleigh number for the onset of convection in a box of aspect ratios h_1, h_2 (ratio of horizontal dimensions to vertical height). The results are summarized in two celebrated figures, one of which is reproduced in figure 1. This shows the horizontal wavevector of the preferred cellular mode (m, n) as a function of h_1, h_2. In the present two-dimensional study we are effectively restricting ourselves to thin three-dimensional boxes with length greater than or equal to the height. For three-dimensional boxes, numerical solutions based on the Galerkin method have been reported by Straus & Schubert (1978, 1979, 1981), Schubert & Straus (1979) and Caltagirone, Meyer & Mojtabi (1981), and based on finite-difference methods by Holst & Aziz (1972) and Horne (1979).

Straus & Schubert (1978) studied the stability of two-dimensional solutions to cross-roll disturbances and delineated the dimensions of those boxes for which the motion is necessarily unsteady or steady and three-dimensional. For example, they found that steady, unicellular, two-dimensional convection cannot exist when the Rayleigh number equals 200 if the ratio of the cylinder length to the dimension of the square vertical cross-section lies between 0.38 and 0.61. Straus & Schubert (1979)

showed that in cubic boxes the flow may be non-unique in that they found two- and three-dimensional steady solutions coexisting for Rayleigh numbers larger than $4.5\pi^2$. This feature was also found by Holst & Aziz (1972) and Horne (1979), who in fact found the co-existence of four solutions: two- and three-dimensional, steady and unsteady. Their solutions also failed to offer support to the Malkus proposition that the flow should evolve to a steady configuration which maximizes the heat transfer: for $Ra < 97$ the two-dimensional flow maximizes heat transfer while for $Ra > 97$ it is the three-dimensional flow. Schubert & Straus (1979) studied the onset of oscillations in two- and three-dimensional, multi-cellular convection in square cavities and cubes, respectively. They found that two-dimensional, unicellular flow becomes time-dependent for $Ra > 300$, but noted that the two-dimensional flows may not be realizable in a three-dimensional box owing to perturbations in the orthogonal direction. Generally the transition occurs at Rayleigh numbers that are in approximate proportion to the number of cells. Straus & Schubert (1981) demonstrated the non-uniqueness of steady, three-dimensional convection in rectangular boxes with square horizontal cross-section. Caltagirone *et al.* (1981) enumerated various stable structures for different Rayleigh numbers and aspect ratios.

By using an analytical eigenfunction-expansion technique and studying the phase-space dynamics of finite-amplitude disturbances. Steen (1983) has been able to compute the probabilities that certain flow patterns will be realized in near-cubic boxes when the system is subjected to random perturbations. He also showed that stable three-dimensional motion in a cube is only possible when $Ra > 4.87\pi^2$. Steen (1985) used the same techniques to consider the effect of container geometry on the transition to unsteady convection. Borkowska-Pawlak & Kordylewski (1985), seemingly unaware of the work of Steen, used a very similar attack in their study of flows near the triple bifurcation point at $Ra = 4.5\pi^2$ for a box of square horizontal cross-section and aspect ratio $= 2^{\frac{1}{2}}$.

To summarize the numerical work: the situation is extremely complex and it is not yet possible to describe fully the multiplicity and stability of the flows that occur, neither is it possible to assign probabilities to the occurrence of flows that have been found. It is known that in cubic boxes the flow is non-unique – it may be two- or three-dimensional, steady or unsteady. The actual flow that is realized in a general box depends critically upon the Rayleigh number and the aspect ratios of the box. By considering thin boxes the flow may be assumed to be steady and two-dimensional, at least for low enough Rayleigh number. Steady two-dimensional flow may exist in other cases, but it is known that certain configurations cannot support it.

The major conclusions are supported by experimental work. Bories, Combarnous & Jaffrennou (1972) using an experimental cell $46.3 \times 66 \times 5.05$ cm high observed three-dimensional polyhedral cells, whilst Caltagirone, Cloupeau & Combarnous (1971) observed fluctuating two-dimensional rolls in a cell 38 cm long, 2 cm wide and 4–6 cm deep. The transition to permanently unsteady motion in the form of two-dimensional rolls was originally found by Combarnous & LeFur (1969) using a cell $37 \times 60 \times 5.5$ cm high. Horne & O'Sullivan (1974) found non-uniqueness in the observed two-dimensional motion inside a Hele-Shaw cell.

The number of numerical investigations into two-dimensional, large amplitude convection is also substantial and we shall not attempt an exhaustive survey. Straus (1974) using a Galerkin technique calculated a balloon-shaped region of Rayleigh number–wavenumber space in which stable solutions exist. Horne & O'Sullivan

(1974) showed the non-uniqueness of the flows in a square cell. Caltagirone (1975) investigated the effect of aspect ratio and also the transition to unsteadiness; this investigation covered the Rayleigh number range 10–2000 and the aspect ratio (width to height) range 0.1–4. Borkowska-Pawlak & Kordylewski (1982) used a truncated Galerkin method to study the transition to oscillatory convection in an infinite layer. They also studied the effect of finite Prandtl–Darcy number.

In independent studies, Aidun & Steen (1987) and Kimura, Schubert & Straus (1987) calculated the transition to oscillatory convection in unicellular flow in two-dimensional square cavities. They found that there exists a Hopf bifurcation at a Rayleigh number of about 390 with a corresponding frequency of about 83 cycles per diffusion time. These calculations are believed to improve on the earlier estimate of the transitional Rayleigh number of 384 ± 5 found by Caltagirone (1975).

It should be emphasized that there is a close analogy between the present porous-medium case and the pure-fluid case which is generally known as the Rayleigh–Bénard problem. There is not a complete equivalence because they possess different symmetry properties. They share $\mathbf{Z}_2 \times \mathbf{Z}_2$ symmetry, but the porous-medium problem possesses in addition a translational invariance so that a two-cell solution in a cavity of aspect ratio 2 is equivalent to a four-cell solution in a cavity of aspect ratio 4, and so on. This translational invariance arises from the slip boundary conditions which apply at the boundaries of the porous medium. In contrast, the no-slip conditions which are appropriate to a pure fluid confined in a cavity destroy the translational invariance.

In terms of simplicity and cost, the present case provides an attractive and viable test-bed for analytical and numerical studies, and the insight gained into the qualitative features of porous-media convection is an invaluable aid to our understanding of the Rayleigh–Bénard problem. From an experimental viewpoint the Rayleigh–Bénard problem does have an advantage in that it is relatively easy to build and operate a Rayleigh–Bénard cell of variable aspect ratio, whereas the porous-media cavities must be repacked in each case.

The numerical techniques that we adopt in this study originate in bifurcation theory, where they have been used mainly for locating singular points in algebraic equations and ordinary differential equations. The basic idea is to extend the set of governing equations with conditions that are satisfied at the bifurcation point to be located. By combining this extended-systems approach with the finite-element approximation, partial differential equations can readily be treated. The approach has been applied with considerable success in the following related studies: flow between concentric rotating cylinders (the Taylor problem) by Cliffe (1983, 1988); buoyancy-driven convection in a fluid heated from below (the Rayleigh–Bénard problem) by Jackson & Winters (1984). The effects of tilt were examined by Cliffe & Winters (1984) and by Winters & Brown (1985) for two- and three-dimensional cavities respectively; flow in a curved tube (the Dean problem) by Winters & Brindley (1984) and Winters (1987*b*); surface-tension-driven convection in a fluid heated from below (the Marangoni problem) by Winters, Plesser & Cliffe (1988); onset of vortex shedding in flow past bluff bodies by Jackson (1987); onset of oscillatory convection in a semiconductor crystal melt and a double-glazing cavity by Winters (1987*a*,*c*); ignition and extinction in a reaction-diffusion system describing thermal explosions by Winters & Cliffe (1985). Some of the above applications to problems in fluid mechanics and heat transfer are summarized by Winters, Cliffe & Jackson (1984, 1987).

The extended systems of equations will be described later, but in anticipation of

their explicit forms we note that we shall be solving basically a linear stability problem to locate the singular points. However, there are several important differences between our approach and more traditional linear stability and weakly nonlinear analyses. First, by solving the extended systems in a finite-element formulation we are able to locate bifurcations in finite regions of arbitrary shape and with arbitrary boundary conditions. Secondly, the idea of solving the basic governing equations simultaneously with conditions satisfied at the singular point establishes a framework for systematically identifying and computing different types of singular points of increasing codimension (Jepson & Spence 1984). Finally, with continuation methods we can follow nonlinear branches which arise at the singular points, we can trace out paths of bifurcation points and we can detect the presence of further bifurcations.

The combination of the extended systems approach with the finite-element approximation gives the present method great generality, allowing the possibility of locating instabilities in more complex configurations, such as the non-planar cases considered by Rees & Riley (1986, 1989*a*,*b*). We note that it is natural in the finite-element method to use a direct solver and this makes available the Jacobian matrix $\boldsymbol{f}_{\boldsymbol{x}}$; this is particular appropriate for bifurcation studies where the Jacobian can be used for parameter continuation (Keller 1977) and for assessing stability.

The plan of the rest of the paper is as follows: in §2 the approximations underlying the problem are discussed and the governing equations are formulated. In §3 analytical and theoretical results are discussed. Linear stability results are first presented and there follows a weakly nonlinear analysis of the modal interaction near the first double eigenvalue at $Ra = 4.5\pi^2$. The expected state diagram is discussed and the effect of varying the aspect ratio is considered. There is then a discussion of the symmetries that the equations possess, and the relationship between the present problem and a Taylor–Couette problem is highlighted. Finally the unfolding with aspect ratio of the double eigenvalue, which arises when the neutral stability curves of the two-cell and six-cell Taylor flows intersect, is outlined. In §4 the equations are cast in a form suitable for numerical solution by the finite-element method. Then we describe the numerical techniques used for locating bifurcation points in the equations and for parameter continuation of the solutions to these equations. In §5 numerical results are presented. Finally in §6 the findings are summarized.

2. Formulation

2.1. *Approximations*

(*a*) The solid matrix is homogeneous, non-deformable and chemically inert with respect to the fluid.

(*b*) The fluid is single phase and Newtonian and under the usual averaging over a representative elementary volume the linear Darcy law results.

(*c*) The Prandtl–Darcy number is large so that the inertia terms may be neglected.

(*d*) The solid and fluid phases are in thermal equilibrium (in certain cases the lack of agreement between theory and experiment has been attributed to the non-validity of this assumption and models have been proposed which include interphase heat transfer coefficients).

(*e*) The relative temperature differences are small enough for the Boussinesq approximation to hold.

(*f*) Thermal dissipation is negligible and an effective (scalar) thermal conductivity may be assumed.

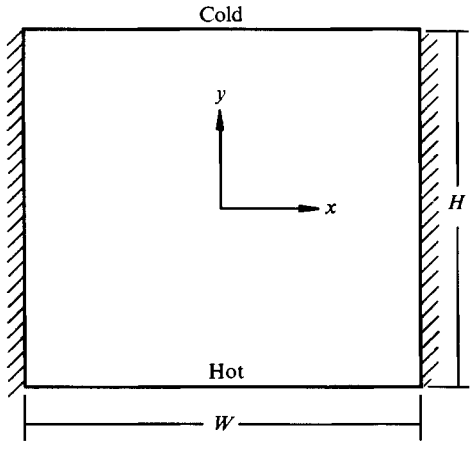

FIGURE 2. The geometry and coordinate system for the two-dimensional rectangular cavity.

2.2. *Problem description*

We consider a two-dimensional rectangular cavity of height H and aspect ratio $h = W/H$, where W is the lateral dimension (width). The cavity (see figure 2) comprises a solid matrix of porosity ϵ', permeability K and heat capacity $(\rho c)_s$, saturated by a fluid with thermal expansion coefficient β, of viscosity ν and heat capacity $(\rho c)_f$. The saturated porous medium is taken to have an effective thermal conductivity k_* and heat capacity $(\rho c)_*$ where

$$(\rho c)_* = \epsilon'(\rho c)_f + (1-\epsilon')(\rho c)_s. \tag{2.1}$$

The lateral boundaries of the cavity are adiabatic, while the upper and lower boundaries are at isothermal temperatures $T_0 - \frac{1}{2}\Delta T$, $T_0 + \frac{1}{2}\Delta$, respectively; ΔT is taken to be positive so that the cavity is heated from below. All boundaries are assumed impermeable.

On invoking the Boussinesq approximation, and assuming that the Prandtl–Darcy number is large, convective flows are governed by the dimensionless equations:

$$\nabla^2\psi = -\frac{Ra}{h}\frac{\partial\theta}{\partial x}, \tag{2.2}$$

$$\nabla^2\theta = \frac{1}{h}\left\{\frac{\partial\psi}{\partial y}\frac{\partial\theta}{\partial x} - \frac{\partial\psi}{\partial x}\frac{\partial\theta}{\partial y}\right\} + \frac{\partial\theta}{\partial t}, \tag{2.3}$$

where (x, y) are Cartesian coordinates based at the centre of the cavity,

$$\nabla^2 = \frac{1}{h^2}\frac{\partial^2}{\partial x^2} + \frac{\partial^2}{\partial y^2},$$

and ψ, θ are stream and temperature functions, respectively. Here Ra denotes the Darcy–Rayleigh number defined by

$$Ra = \frac{g\beta K\Delta T H(\rho c)_f}{\nu k_*} \tag{2.4}$$

and quantities have been non-dimensionalised using lengthscales H or W (as appropriate), diffusive velocity scale $k_*/H(\rho c)_f$ and the temperature scale ΔT.

The governing equations (2.2), (2.3) hold in the region

$$\Omega = \{(x, y): -0.5 < x < 0.5, -0.5 < y < 0.5\}, \tag{2.5}$$

while on the boundaries we have

$$\psi = 0, \quad \frac{\partial \theta}{\partial x} = 0 \quad \text{on } x = \pm\tfrac{1}{2}, |y| < \tfrac{1}{2}, \tag{2.6}$$

$$\psi = 0, \quad \theta = \mp\tfrac{1}{2} \quad \text{on } y = \pm\tfrac{1}{2}, |x| < \tfrac{1}{2}. \tag{2.7}$$

3. Theoretical considerations

3.1. *Lapwood convection*

A linear stability analysis of the pure conduction base state, carried out by Sutton (1970) (who also considered the effect of an imposed weak uniform horizontal flow through the cavity), found that eigenmodes exist when the Rayleigh number satisfies

$$Ra_{m,n} = \frac{\pi^2}{m^2 h^2}(n^2 h^2 + m^2)^2. \tag{3.1}$$

These perturbation eigenmodes represent flows with m horizontal cells and n vertical cells and are given by

$$\Psi_{m,n} = \sin(m\pi\bar{x}) \sin(n\pi\bar{y}), \tag{3.2}$$

$$\Theta_{m,n} = -\frac{1}{Ra_{m,n}^{\frac{1}{2}}} \cos(m\pi\bar{x}) \sin(n\pi\bar{y}), \tag{3.3}$$

where $\bar{x} = x + 0.5$ and $\bar{y} = y + 0.5$. A plot of the linear stability curve (3.1) for various (m, n)-modes is shown in figure 3. The minimum critical Rayleigh number for the (m, n)-mode occurs at aspect ratio $h = m/n$ and is equal to $4\pi^2 n^2$. We note that the lowest critical Rayleigh number for each (m, n)-mode is independent of m. This is a direct consequence of the slip condition on the sidewalls. The same behaviour is found for the Rayleigh–Bénard problem with slip sidewalls, whilst a no-slip condition results in a value of the lowest critical Rayleigh number which varies with the mode. We note further that, whatever the aspect ratio, the mode of lowest critical Rayleigh number always has unit vertical wavenumber, while the corresponding horizontal wavenumber is dependent on the aspect ratio. The wavenumber of this mode changes from $(m, 1)$ to $(m+1, 1)$ at an aspect ratio and Rayleigh number given by

$$h = [m(m+1)]^{\frac{1}{2}}, \quad Ra = \frac{\pi^2(2m+1)^2}{m(m+1)}, \tag{3.4a}$$

and more generally the $(m, 1)$ and $(m', 1)$ modes interchange when

$$h = (mm')^{\frac{1}{2}}, \quad Ra = \frac{\pi^2(m+m')^2}{mm'}. \tag{3.4b}$$

3.2. *Secondary bifurcations: analysis near the first double eigenvalue*

As the aspect ratio increases through one of the critical values given by (3.4*a*),there is an exchange between primary modes, with the mode of lowest critical Rayleigh number changing from $(m, 1)$ to $(m+1, 1)$; in general we shall refer to bifurcations from the trivial branch as primary bifurcations. This type of exchange has been discussed in a general qualitative way by Schaeffer (1980): it is now well understood

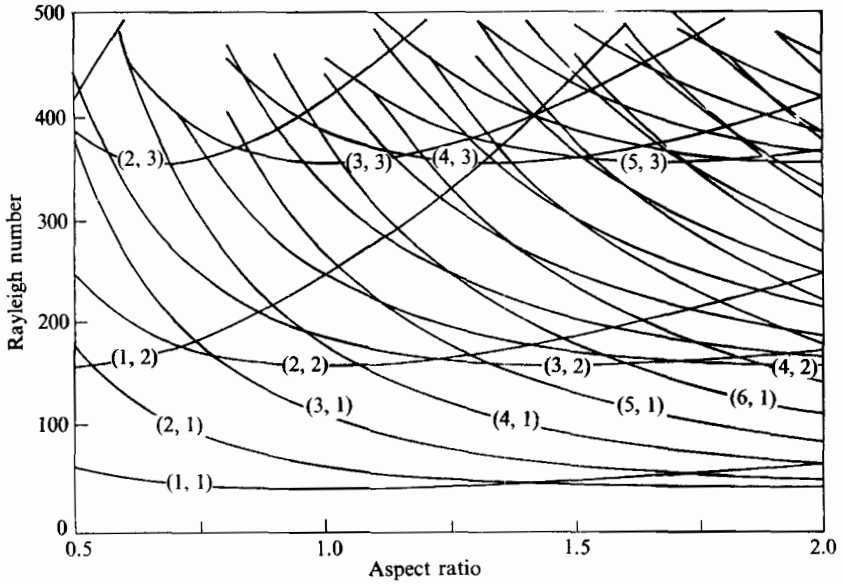

FIGURE 3. The variation of critical Rayleigh number with aspect ratio for the lower modes in Lapwood convection.

(see Shearer 1980) that this exchange process between solutions both of which possess $\mathbf{Z}_2$ symmetry is often associated with secondary bifurcations (that is bifurcations from a primary branch) which transfer from one modal solution branch to the other as the exchange takes place. The qualitative picture of the Schaeffer nine-solution branch mechanism is illustrated in figure 4. Basically the secondary bifurcations are required to satisfy constraints on the Leray–Schauder degree of the solution branches, whilst ensuring that the degrees are consistent as $Ra \to \infty$. In an earlier paper Bauer, Keller & Reiss (1975) discussed examples involving multiple eigenvalues and showed that weakly nonlinear theory may be applied to analyse the local structure as the exchange takes place. The theory was subsequently employed by Kidachi (1982) to investigate the primary mode interchange in the Rayleigh–Bénard problem with idealized slip boundary conditions on the sidewalls; Metzener (1986) extended this work to the no-slip case. Here, in order to check our numerical results and to investigate the nature of the secondary bifurcations, we employ weakly nonlinear theory to investigate the interaction between the (1, 1) and (2, 1) primary modes. The expected paths of bifurcation points in the (h, Ra)-plane are illustrated schematically for this case in figure 5. We are concerned with the solution near to the double eigenvalue $Ra = Ra_c = 4.5\pi^2$ which occurs when $h = \sqrt{2}$ and we are thus led to seek solutions to (2.2) and (2.3) subject to (2.6) and (2.7) in the form

$$\psi = \epsilon\psi_0 + \epsilon^2\psi_1 + \ldots, \tag{3.5}$$

$$\theta = -y + \epsilon\theta_0 + \epsilon^2\theta_1 + \ldots, \tag{3.6}$$

$$h = \sqrt{2}(1 + \tfrac{1}{2}\epsilon^2\Delta + \ldots), \tag{3.7}$$

$$Ra = Ra_c(1 + \epsilon^2 R_1 + \ldots), \tag{3.8}$$

with $\Delta = \text{sign}(h - \sqrt{2})$ and where ψ_i, θ_i are functions of x, y and the slow timescale $\tau = \epsilon^2 t$.

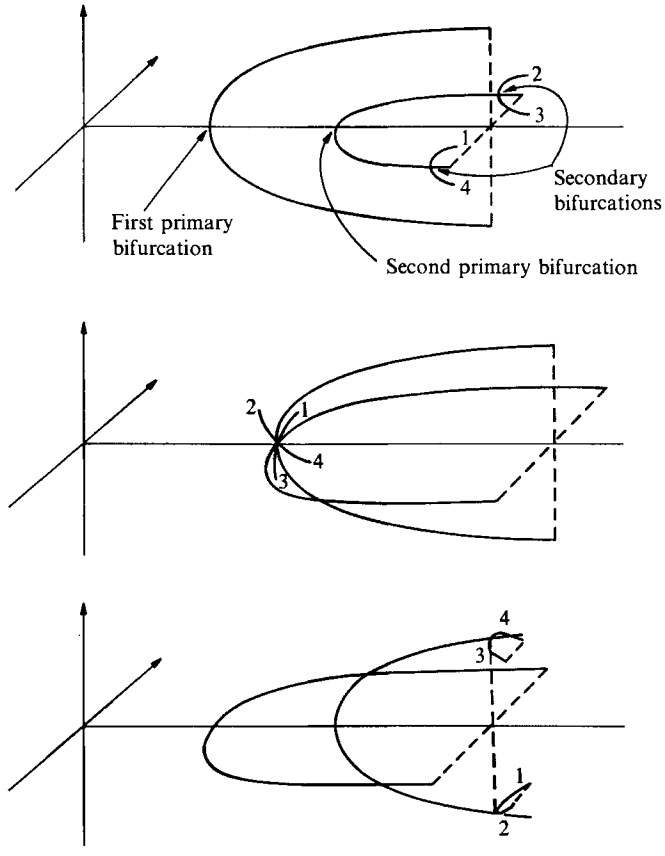

FIGURE 4. Schematic illustration of the role of secondary bifurcations in the primary-mode exchange that occurs as the aspect ratio increases.

Proceeding in the standard fashion and omitting all detail we find that

$$(\psi_0, \theta_0) = A(\tau)(\Psi_{1,1}, \Theta_{1,1}) + B(\tau)(\Psi_{2,1}, \Theta_{2,1}), \tag{3.9}$$

where $A(\tau)$, $B(\tau)$ are the amplitudes of the (1, 1) and (2, 1) modes respectively. Applying solvability conditions to the $O(\epsilon^3)$-equations yields the evolution equations for the amplitudes:

$$\frac{\mathrm{d}A}{\mathrm{d}\tau} = \tfrac{1}{16}\pi^2 A\{d_1 - A^2 - c_1 B^2\}, \tag{3.10}$$

$$\frac{\mathrm{d}B}{\mathrm{d}\tau} = \tfrac{1}{4}\pi^2 B\{d_2 - c_2 A^2 - B^2\}, \tag{3.11}$$

with $$c_1 = 5, \quad c_2 = \tfrac{7}{8}, \quad d_1 = 8\{3R_1 - \Delta\}, \quad d_2 = 4\{3R_1 + \Delta\}. \tag{3.12}$$

The equations possess three solutions which do not depend upon the interaction of the (1, 1) and (2, 1) modes; these are

(i) $A = B = 0$ (trivial mode), (3.13*a*)

(ii) $B = 0$, $A^2 = d_1$, $d_1 > 0$ (pure (1, 1) mode), (3.13*b*)

(iii) $A = 0$, $B^2 = d_2$, $d_2 > 0$ (pure (2, 1) mode). (3.13*c*)

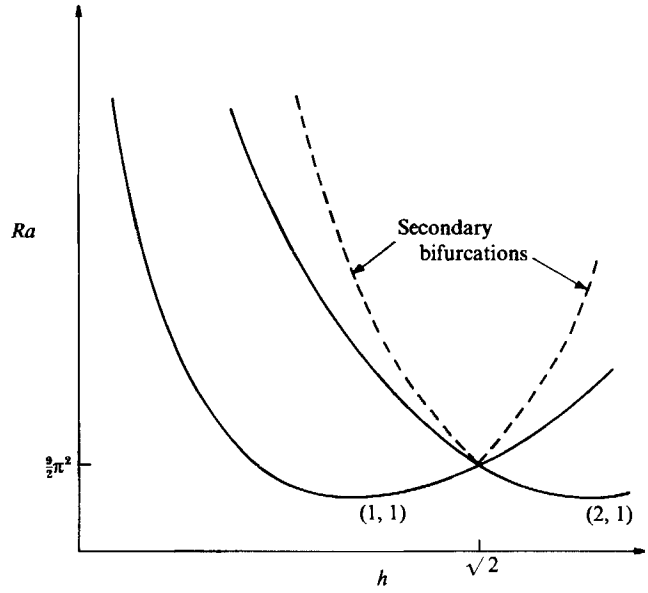

FIGURE 5. Schematic illustration of the expected variation of the critical Rayleigh numbers of the primary (full curves) and secondary bifurcations (broken curves) with aspect ratio.

The amplitude of the disturbance is zero for $Ra < \min\{Ra_1, Ra_2\}$, where

$$Ra_1 = 1.5\pi^2(1+\sqrt{2}h), \quad Ra_2 = 1.5\pi^2(5-\sqrt{2}h),$$

but bifurcates at Ra_1 and Ra_2. These bifurcated solutions suffer secondary bifurcations because of the presence of mixed-mode solutions in which neither A nor B is zero. These solutions are given by

$$\left.\begin{aligned} A^2 &= \frac{c_1 d_2 - d_1}{c_1 c_2 - 1}, \quad c_1 d_2 - d_1 > 0, \\ B^2 &= \frac{c_2 d_1 - d_2}{c_1 c_2 - 1}, \quad c_2 d_1 - d_2 > 0. \end{aligned}\right\} \tag{3.13d}$$

It is a straightforward matter to determine the stability of the various solutions to small disturbances and we omit the detail.

The results of the above analysis are summarized in figures 6. In figure 6(*a*) we present a perspective view of the situation that obtains when $h < \sqrt{2}$. We see that the (1, 1) mode, given by (3.13*b*), bifurcates from the trivial solution at $Ra = Ra_1$; this primary branch is stable. At $Ra = Ra_2$ there is a further primary bifurcation to the (2,1) mode given by (3.13*c*) and this mode undergoes secondary bifurcation at $Ra = Ra_3$, where

$$Ra_3 = 0.5\pi^2(23 - 7\sqrt{2}h).$$

The (2,1) mode is unstable for $Ra < Ra_3$ but is stabilized by the secondary bifurcation. As $h \to \sqrt{2}$, $(Ra_1, Ra_2) \to Ra_c$ and the first and second primary branches approach each other, with the range of Rayleigh number for which the second primary is unstable diminishing. At $h = \sqrt{2}$, all the bifurcation points coincide with the pure modes completely stable and the mixed modes unstable (figure 6*b*). As h increases further the branches separate again with the (2, 1) mode becoming the leading primary and with the mixed mode now bifurcating off the (1, 1) mode. This

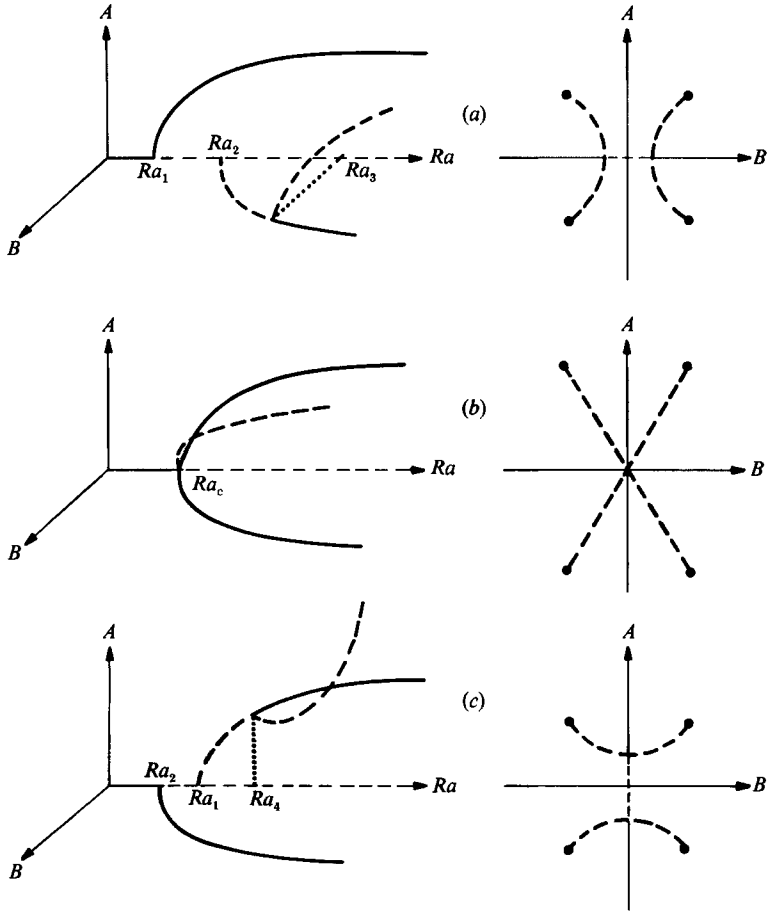

FIGURE 6. Variation with Rayleigh number of the amplitudes of the (1, 1) and (2, 1) modes (A and B respectively). End-on views along the Ra-axis are shown to the right. Stable/unstable branches are denoted by full/dashed curves respectively. (*a*) $h < \sqrt{2}$, (*b*) $h = \sqrt{2}$, (*c*) $h > \sqrt{2}$.

situation is shown in figure 6 (*c*): the (2, 1) mode bifurcates at $Ra = Ra_2$, the (1, 1) mode at $Ra = Ra_1$. The secondary bifurcation now occurs at $Ra = Ra_4$, where

$$Ra_4 = 0.5\pi^2(11\sqrt{2}h - 13),$$

leaving the primary mode stable as before.

In figure 6 we also display the 'end-on' view along the length of the Rayleigh number axis in order to clarify the shape of the secondary bifurcation branches. Note that the secondary branches actually continue out to infinity but are truncated in the figures.

3.3 *Symmetries*

It is straightforward to show that the governing system of steady equations possesses $\mathbf{Z}_2 \times \mathbf{Z}_2$ symmetry, where the generators of the group are S_x, S_y defined by

$$S_x\begin{pmatrix}\psi\\ \theta\end{pmatrix} = S_x\begin{pmatrix}\psi(x,y)\\ \theta(x,y)\end{pmatrix} = \begin{pmatrix}-\psi(-x,y)\\ +\theta(-x,y)\end{pmatrix}, \tag{3.14}$$

$$S_y\begin{pmatrix}\psi\\ \theta\end{pmatrix} = S_y\begin{pmatrix}\psi(x,y)\\ \theta(x,y)\end{pmatrix} = \begin{pmatrix}-\psi(x,-y)\\ -\theta(x,-y)\end{pmatrix}. \tag{3.15}$$

The representation Γ' of the group $\mathbf{Z}_2 \times \mathbf{Z}_2$ is $\Gamma' = \{I, S_x, S_y, S_x S_y\}$, where I is the identity operator. Here S_x, S_y and $S_x S_y$ represent left-right, up-down and centro-symmetries, respectively.

There exists a solution representing a pure conduction state, viz. $\theta = -y$, $\psi = 0$, for all Ra, and the bifurcations from this trivial solution will have distinct symmetry properties depending on the number of horizontal cells m and vertical cells n. A bifurcation to an odd number of cells in direction i ($i = x$ or y) breaks the symmetry S_i, whilst if $|m-n|$ is odd then the centro-symmetry $S_x S_y$ is broken. Table 1 illustrates the combinations that arise in practice.

In addition to these symmetries the slip condition (2.6) implies a translational invariance. The simplest description of this invariance is obtained by embedding the physical cell in an infinite, periodic array of cells in the x-direction. Then the (m, n)-mode possesses translational symmetries T_m^p, where $p = 1, 2, \ldots, m-1$ and

$$T_m^p \begin{pmatrix} \psi \\ \theta \end{pmatrix} = T_m^p \begin{pmatrix} \psi(x,y) \\ \theta(x,y) \end{pmatrix} = \begin{pmatrix} \psi\left(x + \frac{2p}{m}, y\right) \\ \theta\left(x + \frac{2p}{m}, y\right) \end{pmatrix}. \tag{3.16}$$

This symmetry has an important consequence for the crossing of paths of bifurcation points (which was alluded to in §3.1). The point at which two paths cross is a double eigenvalue and normally a double eigenvalue in a problem with $\mathbf{Z}_2 \times \mathbf{Z}_2$ symmetry is not structurally stable if each path breaks the same symmetry (Cliffe & Winters 1986). In fact structural stability only occurs for a special value of a further parameter; the double eigenvalue is a codimension-1 singularity. In contrast, if the paths break *different* symmetries then they will always cross. In Lapwood convection, the translational symmetry arising from the slip condition guarantees that all paths will cross.

The (1, 1) and (2, 1) modes both have $\mathbf{Z}_2$ symmetry with group generators $S_x S_y$ and S_x, respectively. Thus their exchange is governed by the Shaeffer nine-solution-branch model, which is illustrated qualitatively by figure 4. For $h \sim 1$, the one-cell (1, 1) primary mode, which being an odd-cell mode breaks the S_x and S_y symmetries, bifurcates first. Then at higher Rayleigh number the two-cell (2, 1) mode, which breaks the S_y and $S_x S_y$ symmetries bifurcates. As the aspect ratio increases these primary branches swap over and, as described in §3.2, the exchange of primary modes is accompanied by a transfer of a secondary bifurcation. The secondary bifurcation from the two-cell branch at $h \sim 1$ breaks the S_x symmetry, but at larger h the secondary bifurcation from the one-cell branch breaks the centro-symmetry. This is possible only because all symmetries have been broken.

The exchange of the (1, 1) and (3, 1) modes, however, is more complicated. The modes both have $\mathbf{Z}_2$ symmetry, but with the same group generator $S_x S_y$; thus the Schaeffer model does not apply. In fact, the one-cell mode is invariant with respect to $\{I, S_x S_y\}$ and the three-cell with respect to $\{I, S_x S_y, T_3^1, T_3^2\}$. Thus the modes possess effectively the same symmetry groups found by Tavener & Cliffe (1988) for the two-cell/six-cell interchange in the Taylor–Couette flow problem with impermeable, stress-free end-cap conditions.

3.4. *The Taylor–Couette two-cell six-cell interchange model*

The flow considered by Tavener & Cliffe is that of an incompressible, viscous fluid between two concentric cylinders, with the inner one rotating and the outer one fixed.

Mode	Symmetries broken
(1, 1)	S_x, S_y
(2, 1)	$S_y, S_x S_y$
(1, 2)	$S_x, S_x S_y$
(2, 2)	none

TABLE 1

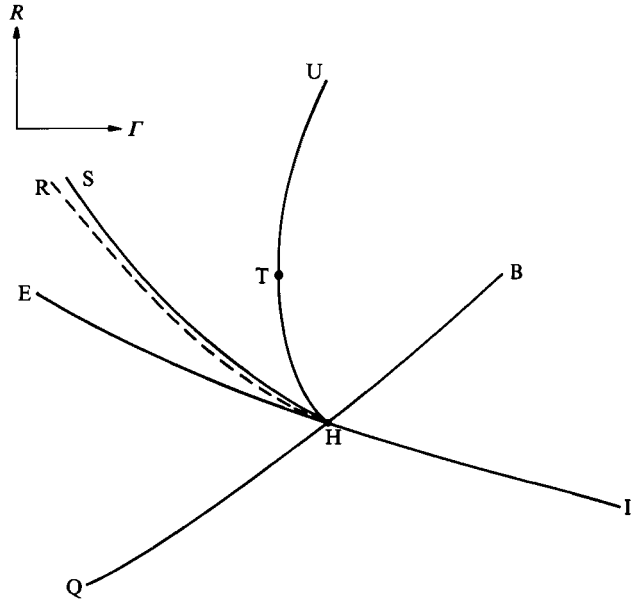

FIGURE 7. Loci of singular points in the Taylor–Couette problem. Here Γ and R denote respectively the aspect ratio and rotation Reynolds number.

The length of the cylinders is finite and the end caps are assumed to be impermeable and stress free. In this Taylor problem cellular flows bifurcate from a trivial Couette flow solution. Using symmetry arguments and numerical bifurcation techniques Tavener & Cliffe analysed the modal exchanges which take place between two-, four- and six-cell flows as the length of the cylinder increases with the gap width fixed (or, more generally, as the aspect ratio changes).

In terms of the underlying symmetries, it is the two- six-cell interchange which corresponds to the one- three-cell interchange in the porous-medium problem considered in this paper. The results concerning the two- six-cell interchange are summarized in figures 7 and 8. In figure 7, the neutral stability curves along which the Couette flow loses stability with respect to two-cell and six-cell flows are labelled QHB and EHI, respectively. The loss of stability in each case is associated with a loss of translational invariance and occurs at a pitchfork bifurcation point, which is supercritical in the neighbourhood of the modal exchange. Secondary bifurcation on the six-cell branches occurs along the locus of transcritical bifurcation points SH in figure 7; this bifurcation is also associated with a loss of translational invariance and is subspace breaking. The associated locus of limit points, RH, lies close to SH. At a critical length, the branches arising from the secondary bifurcation points on the six-cell branches become connected to the two-cell branches at the transcritical

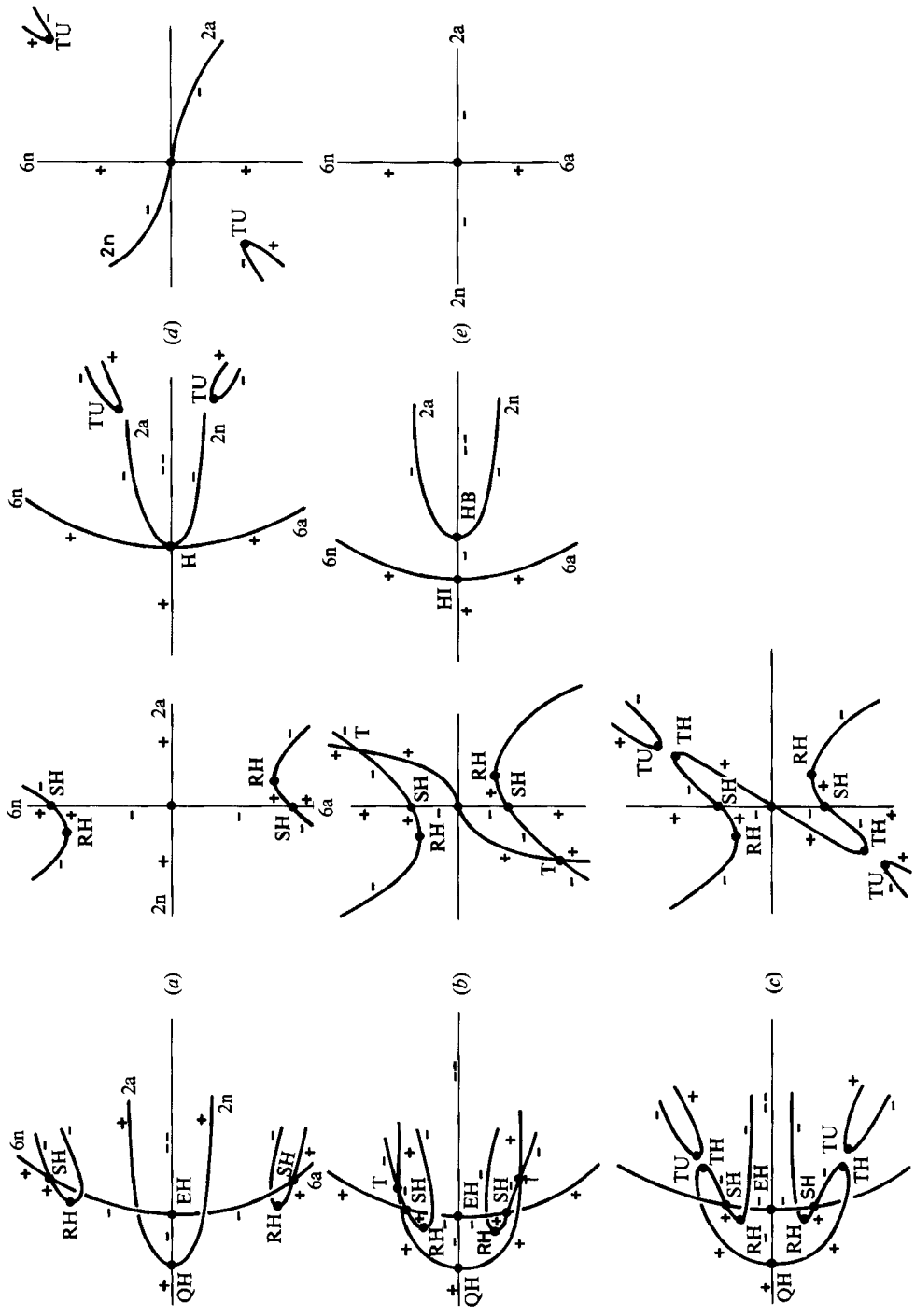

FIGURE 8. Schematics of state diagrams for two-cell/six-cell interchange in the Taylor–Couette problem. (*a*) $\Gamma < \Gamma_{\mathrm{T}}$, (*b*) $\Gamma = \Gamma_{\mathrm{T}}$, (*c*) $\Gamma_{\mathrm{T}} < \Gamma < \Gamma_{\mathrm{H}}$, (*d*) $\Gamma = \Gamma_{\mathrm{H}}$, (*e*) $\Gamma > \Gamma_{\mathrm{H}}$.

bifurcation point T. Two paths of limit points result when this transcritical bifurcation disconnects in the opposite sense. The locus of limit points on the continuous branch connecting two- and six-cell flows is labelled TH. The limit points indicating the lower stability limit of a pair of disconnected two-cell flows are labelled TU.

In figure 8(*a*) the two-cell flows bifurcate from the trivial solution at a lower Reynolds number than the six-cell flows. The branches are lettered according to the direction of flow at the end caps: a/n denotes the flow which is inwardly/outwardly spiralling at the ends. At a critical length, figure 8(*b*), the branches arising at secondary transcritical bifurcations on the six-cell branches connect with the two-cell flow branches, such that the branches *a* and *n* cross. The transcritical bifurcations T and the limit points RH occur on either side of the secondary bifurcations SH. As the length increases further, the transcritical bifurcations T disconnect, producing a continuous, folded branch connecting the two-cell and six-cell flows, as shown in figure 8(*c*). The limit points RH and TH, the secondary bifurcation points SH and the primary bifurcation points QH and EH coalesce at the double singular point H, figure 8(*d*). As the length increases further, the primary bifurcation points QH and EH emerge from the double singular point H in the opposite order as HB and HI, and the branches swap stability, figure 8(*e*).

4. Numerical methods

4.1. *Finite-element equations*

The equations (2.2) and (2.3) are discretized in the finite-element approximation using a standard Galerkin formulation with the second-order terms integrated by parts. This leads to the following form:

$$\int_\Omega f_\psi Ra\left\{\frac{\partial\theta}{\partial y}\sin\phi-\frac{1}{h}\frac{\partial\theta}{\partial x}\cos\phi\right\}+\int_\Omega\left(\frac{1}{h^2}\frac{\partial f_\psi}{\partial x}\frac{\partial\psi}{\partial x}+\frac{\partial f_\psi}{\partial y}\frac{\partial\psi}{\partial y}\right)-\int_{\Gamma_\psi} f_\psi\frac{\partial\psi}{\partial n}=0, \tag{4.1}$$

$$\int_\Omega f_\theta\left\{\frac{1}{h}\left(\frac{\partial\psi}{\partial y}\frac{\partial\theta}{\partial x}-\frac{\partial\psi}{\partial x}\frac{\partial\theta}{\partial y}\right)+\frac{\partial\theta}{\partial t}\right\}+\int_\Omega\left(\frac{1}{h^2}\frac{\partial f_\theta}{\partial x}\frac{\partial\theta}{\partial x}+\frac{\partial f_\theta}{\partial y}\frac{\partial\theta}{\partial y}\right)-\int_{\Gamma_\theta} f_\theta\frac{\partial\theta}{\partial n}=0. \tag{4.2}$$

In the above equations: Ω is the spatial region being discretized; Γ is the boundary of Ω; Γ_ψ is the part of Γ with no specified value for ψ; Γ_θ is the part of Γ with no specified value for θ; f_ψ is a test function for the variable ψ which is zero on $\Gamma-\Gamma_\psi$; f_θ is a test function for the variable θ which is zero on Γ-Γ_θ; $\boldsymbol{n}$ is the outward normal at the boundary.

In locating non-trivial bifurcations which break the reflectional symmetries the numerical techniques make use of an unfolding parameter which itself breaks those symmetries. Physically, the most natural way of breaking these symmetries is by tilting the cavity so that the isothermal surfaces are no longer perpendicular to the gravity vector. We adopt this method here and introduce the parameter ϕ, the angle of inclination of the hot surface to the horizontal (measured in a clockwise sense). This formulation also accommodates the study of convection in a tilted rectangular cavity, see Riley & Winters (1986, 1987), which is itself important.

The integration by parts gives a boundary integral for each equation over that part of Γ for which a specified value is not set for the corresponding variable. The integrand consists of a normal flux and the boundary integral contributes only when this flux is non-zero. For the present boundary conditions (2.6) and (2.7) all boundary integrals are zero.

In our finite-element approximation of these weak equations we expand the stream function and temperature in quadratic functions based on nine-noded quadrilateral elements. A Galerkin formulation is adopted in which the test functions f_ψ and f_θ are chosen from the same set of quadratic basis functions. The resulting integrals of products of quadratic functions are evaluated numerically by Gauss quadrature. The nonlinear algebraic equations for the unknown nodal values of stream function and temperature are linearized using a Newton–Raphson procedure, and the solution of the linear set of equations at each iteration is obtained using a direct, frontal solver.

4.2. *Bifurcation algorithms*

We write the set of nonlinear algebraic equations which result from the finite-element discretization of (4.1) and (4.2) as

$$\mathrm{M}\frac{\partial \boldsymbol{x}}{\partial t} + \boldsymbol{f}(\boldsymbol{x}, \lambda, \boldsymbol{a}) = \boldsymbol{0} \quad (\boldsymbol{x} \in \boldsymbol{X}), \tag{4.3}$$

where $\boldsymbol{f}$ is a smooth nonlinear function, M is a linear operator on $\boldsymbol{X}$ ($\boldsymbol{R}^n$ in this case, where n is the number of degrees of freedom in the discretization), λ is a bifurcation parameter, and $\boldsymbol{a}$ is a vector of control parameters. We distinguish the bifurcation parameter λ from the control parameters $\boldsymbol{a}$ because we seek the change of behaviour as this particular parameter is varied.

In the present problem we are concerned only with steady-state solutions of (4.3), that is solutions $\boldsymbol{x}$ which satisify:

$$\boldsymbol{f}(\boldsymbol{x}, \lambda, \boldsymbol{a}) = \boldsymbol{0}, \tag{4.4}$$

and we wish to locate the critical values of λ at which bifurcations in the solutions occur. Here, the bifurcation parameter is the Rayleigh number Ra and the control parameters are the aspect ratio h and the tilt ϕ. Our first objective will be to locate these bifurcations in an untilted cavity for fixed values of the control parameter h. Having located a singular point we shall then obtain the variation of the critical bifurcation parameter Ra as h varies. In this way a path of bifurcation points is traced out, and this path may itself have a singular point that we wish to locate.

To understand how we are able to obtain information on possible bifurcations and instabilities from the steady-state equations, we consider the linear stability of a steady solution $\boldsymbol{x}_0$ of equation (4.4) with respect to a small perturbation $\boldsymbol{x}_1$. The behaviour of the perturbation $\boldsymbol{x}_1$ is governed to lowest order by the linear equation

$$\mathrm{M}\frac{\partial \boldsymbol{x}_1}{\partial t} + \boldsymbol{f}_x(\boldsymbol{x}_0, \lambda, \boldsymbol{a})\,\boldsymbol{x}_1 = \boldsymbol{0}. \tag{4.5}$$

Now let $\boldsymbol{\chi}$ be a generalized eigenvector of $\boldsymbol{f}_x(\boldsymbol{x}_0, \lambda, \boldsymbol{a})$ with eigenvalue σ such that

$$\boldsymbol{f}_x \boldsymbol{\chi} = \sigma \mathrm{M} \boldsymbol{\chi}. \tag{4.6}$$

Then if the perturbation $\boldsymbol{x}_1$ is along $\boldsymbol{\chi}$ it behaves as

$$\boldsymbol{x}_1(t) = \epsilon \mathrm{e}^{-\sigma t} \boldsymbol{\chi}, \tag{4.7}$$

where ϵ is the component of $\boldsymbol{x}_1$ along $\boldsymbol{\chi}$ at $t = 0$. The steady solution $\boldsymbol{x}_0$ is linearly stable if all the generalized eigenvalues σ have $\mathrm{Re}\,(\sigma) > 0$; all small perturbations

will decay until the steady state is restored. We note that since $\boldsymbol{f}_x$ is real the eigenvalues in (4.6) are either real or else occur in complex-conjugate pairs.

As the bifurcation parameter λ varies, the linear stability of the steady solution $\boldsymbol{x}_0$ changes when one or more eigenvalues in (4.6) cross the imaginary axis. Thus there is a critical value of λ for which $\sigma = 0$ and $\boldsymbol{f}_x$ is singular; this critical value is called a singular or bifurcation point of equation (4.4). We know from the implicit function theorem that the uniqueness of the steady solution $\boldsymbol{x}_0$ cannot be guaranteed when the Jacobian $\boldsymbol{f}_x$ becomes singular and this usually (but not necessarily) marks the appearance of multiple steady-state solutions.

We note that if a generalized eigenvalue becomes purely imaginary, that is $\sigma = \pm \mathrm{i}\omega$, then (4.4) has a Hopf bifurcation which gives rise to periodic solutions of angular frequency ω at a critical value of λ, although the Jacobian $\boldsymbol{f}_x$ is not actually singular at that point. The existence of Hopf bifurcations in the present problem will be studied in a future paper.

4.2.1. *Stability of solution branches*

From the above discussion it might appear that the stability of solution branches can be deduced only from a computation of the full eigenvalue spectrum of $\boldsymbol{f}_x$. Fortunately, limited information on stability can be inferred from the Jacobian determinant: since this is the product of the eigenvalues then its sign must equal $(-1)^n$, where n is the number of negative, unstable eigenvalues. Thus, a negative sign indicates that the branch is unstable since there is at least one negative eigenvalue, but a positive sign does not imply stability since there might be an even number of unstable eigenvalues. The sign of the Jacobian determinant is also useful for detecting bifurcation points along a solution branch whilst varying the bifurcation parameter λ, since the sign will in general change when a singular point is passed.

4.2.2. *Extended systems*

The general procedure we adopt for locating bifurcation points of equation (4.4) is to solve the equation simultaneously with conditions satisfied at the bifurcation. One condition which must always hold, by definition, is that the Jacobian matrix is singular so that it has at least one zero eigenvalue. Additional conditions may hold depending on the type of bifurcation which is to be located and these conditions can be derived from singularity theory (Golubitsky & Schaeffer 1985). The resulting extended system of equations is solved by Newton's method to give both the solution at the bifurcation point and the value of the bifurcation parameter. This approach is described in detail in Jepson & Spence (1984).

The different types of bifurcations which occur in the present problem are: primary bifurcations which are symmetry-breaking bifurcation points from a trivial solution; secondary bifurcations which may be either symmetry-breaking bifurcation points or transcritical bifurcations from a non-trivial solution; limit points arising from the unfolding of both primary and secondary bifurcations.

4.2.3. *Primary bifurcations from the trivial branch*

In the present problem the majority of primary bifurcations are of a special type of symmetry-breaking bifurcation in which the branching occurs from a trivial solution, namely the conducting, no-flow state which exists for all values of the Rayleigh number. We define a trivial solution of equation (4.4) to be a solution that is independent of λ and denote it $\boldsymbol{x}_0$: We locate bifurcations from $\boldsymbol{x}_0$ by computing

the eigenvectors ξ of the Jacobian matrix $\boldsymbol{f}_x(\boldsymbol{x}_0, \lambda, \boldsymbol{a})$ which have a simple zero eigenvalue, that is we solve

$$\boldsymbol{f}_x(\boldsymbol{x}_0, \lambda, \boldsymbol{a})\,\xi = \boldsymbol{0} \tag{4.8}$$

$$l(\xi) - 1 = 0, \tag{4.9}$$

where (4.9) defines a normalization for the right eigenvector ξ.

The branch of solutions bifurcating away from the singular point $(\boldsymbol{x}_0, \lambda_0, \boldsymbol{a})$ may be approximated by

$$\boldsymbol{x} = \boldsymbol{x}_0 + \epsilon\xi_0 + \ldots, \tag{4.10}$$

$$\lambda = \lambda_0 + \tfrac{1}{2}\epsilon^2\delta + \ldots, \tag{4.11}$$

where δ is defined by a complex expression given by Winters *et al.* (1988).

The above expressions reflect the fact that the primary bifurcations are pitchfork in shape. They will be either sub-or super-critical according to whether δ is negative or positive.

In order to compute the solution on any nonlinear branch which bifurcates from the trivial solution we use (4.10) and (4.11) to construct an initial guess at the new value of λ; Newton's method will then converge quadratically to the solution on the branch for sufficiently small $(\lambda - \lambda_0)$. The branch is then followed for varying λ by standard continuation techniques (see §4.2.6).

4.2.4. *Secondary bifurcations*

The secondary bifurcations are singular points on solution branches which themselves have arisen at primary bifurcations. In the present problem they are either symmetry-breaking or subspace-breaking bifurcations and by definition they always branch from a non-trivial solution.

Considering first the bifurcations that are subspace breaking, these will be transcritical since this is the general form of a bifurcation which does not break any symmetry. To locate a transcritical bifurcation we use the extended system proposed by Moore & Spence (1980) for locating limit points:

$$\boldsymbol{f}(\boldsymbol{x}, \lambda, \boldsymbol{a}) = 0, \quad \boldsymbol{f}_x(\boldsymbol{x}, \lambda, \boldsymbol{a})\,\xi = 0, \quad l(\xi) - 1 = 0, \tag{4.12}$$

and we solve this together with the additional condition (Jepson & Spence 1984)

$$\eta \boldsymbol{f}_\lambda(\boldsymbol{x}, \lambda, \boldsymbol{a}) = 0, \tag{4.13}$$

where η is the left eigenvector of the Jacobian matrix. This algorithm locates the critical values of *two* parameters at which there is a transcritical bifurcation in the steady equations (4.4). The first of these parameters is the bifurcation parameter λ and the second can be any one of the control parameters $\boldsymbol{a}$ provided that the effect of varying that parameter is to unfold the bifurcation. This second parameter is the tilt ϕ for subspace-breaking bifurcations.

Turning next to the secondary bifurcations which are symmetry breaking, we have seen in §3 that two main types are expected: (i) a secondary bifurcation from a branch which will break the remaining reflection symmetry S_x; (ii) a secondary bifurcation from a branch which will break the remaining centro-symmetry $S_x S_y$. Since the reflection symmetry is lost when the cavity is tilted, the first type can be computed as a transcritical bifurcation with ϕ as the unfolding parameter, as discussed above. The location of the second type is problematic since centro-symmetry is not lost when the cavity is tilted so that the bifurcation is not unfolded by varying ϕ. We overcome this by introducing a perturbation into (2.2) and (2.3) which breaks the centro-symmetry and let the amplitude of this perturbation be the

unfolding parameter in applying the extended system for the transcritical bifurcation.

4.2.5. *Limit points*

A limit point (often called a turning point or a one-sided bifurcation point) arises in the present problem during the (3, 1) and (1, 1) modal exchange. We located limit points using the extended system (4.12) of Moore & Spence (1980) described above.

4.2.6. *Continuation*

Euler–Newton continuation is an effective means of following a particular solution branch. In its simplest form the solution $\boldsymbol{x}_0$ obtained at $\lambda = \lambda_0$, and its derivative $\partial \boldsymbol{x}_0/\partial\lambda$, are used to predict the solution $\boldsymbol{x}_1$ at a new value λ_1, from

$$\boldsymbol{x}_1 = \boldsymbol{x}_0 + \frac{\partial \boldsymbol{x}_0}{\partial \lambda}(\lambda_1 - \lambda_0). \tag{4.14}$$

The Newton–Raphson iterations converge rapidly at each value of λ, for a suitable step size $(\lambda_1 - \lambda_0)$, but this procedure ultimately fails at a limit point in the solution curve, where the Jacobian matrix is singular.

In practice, we used a better method which introduces a pseudo-arclength parameter, s, to parametrize the solution (Keller 1977). For continuation in $\lambda = \lambda(s)$ we solve the extended system

$$\boldsymbol{f}(\boldsymbol{x}, \lambda, \boldsymbol{a}) = 0, \quad N(\boldsymbol{x}, \lambda, s) = 0, \tag{4.15}$$

where

$$N = \left[\frac{\partial \boldsymbol{x}}{\partial s}(s_0)\right]^T [\boldsymbol{x}(s) - \boldsymbol{x}(s_0)] + \frac{\partial \lambda}{\partial s}(s_0)[\lambda(s) - \lambda(s_0)] - (s - s_0). \tag{4.16}$$

With Euler–Newton continuation in s rather than λ, it is possible to follow the solution around a limit point, since the Jacobian matrix of system (4.15) and (4.16) is non-singular. The presence of a symmetry-breaking bifurcation point or limit point is determined by monitoring the Jacobian determinant, which changes sign as the singular point is passed.

Paths of singular points were traced by applying continuation in h or ϕ to the appropriate extended system, augmented in the manner of equation (4.15).

5. Computations

All computations were carried out on the CRAY-1S and CRAY-XMP at Harwell using the finite-element code ENTWIFE. Our aim in this study was to resolve the bifurcation structure. To this end we carried out grid-independence and accuracy checks on certain critical values; see table 2, for example. We endeavoured to ensure that we did not introduce spurious bifurcation through the use of too coarse a grid, but we did not perform grid-independence checks on the predicted flows at the highest Rayleigh numbers considered.

5.1. *The state diagram and flows at $h = 1$*

Figure 9 shows the computed bifurcation structure when $h = 1$ and for Rayleigh numbers up to 100. The measure used in all computed state diagrams is the left-hand midwall temperature and, in accord with standard practice, the solid and dashed lines indicate stable and unstable branches respectively. The secondary bifurcations which stabilize the two-cell mode occur at a Rayleigh number of 81.01. As a result,

Mode (m,n)	Critical Rayleigh number: Analytical		Numerical	Grid
(1, 1)	$4\pi^2$	(= 39.478)	39.481	8×8
			39.518	4×4
(2, 1)	$\frac{25}{4}\pi^2$	(= 61.685)	61.736	8×8
			61.432	4×4
(3,1)	$\frac{100}{9}\pi^2$	(= 109.66)	110.15	8×8
(2,2)	$16\pi^2$	(= 157.91)	158.07	8×8
(4,1)	$\frac{289}{16}\pi^2$	(= 178.27)	180.79	8×8

TABLE 2

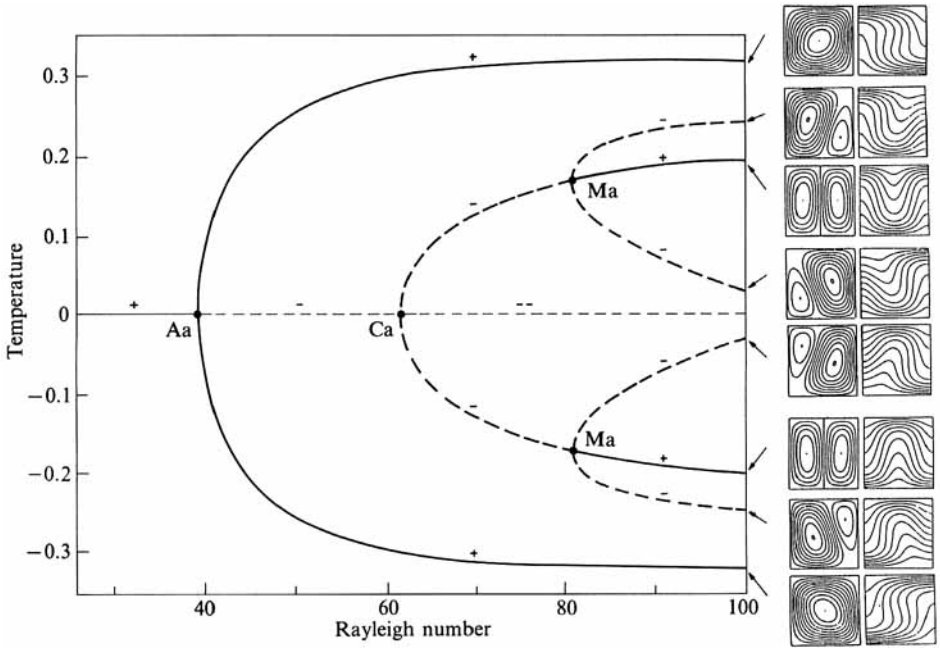

FIGURE 9. Computed bifurcation structure at unit aspect ratio. A plus sign denotes that all the eigenvalues of the Jacobian matrix are positive. If negative eigenvalues exist then their number is indicated by the number of negative signs on the branch. The measure used is the temperature at $(-0.5, 0.0)$. The insets show the streamlines (left) and isotherms (right) at $Ra = 100$. The contour levels are equally spaced between the maximum and minimum values of the stream function and temperature.

for Rayleigh numbers in excess of this critical value both stable one-cell and two-cell modes exist. In theory either mode may be observed, but the one-cell mode will be preferred and the two-cell mode will be anomalous under conditions where the Rayleigh number is raised by gradually increasing the applied temperature difference. Information regarding the eigenvalues of the Jacobian matrix is given along the various solution branches: a plus sign indicates that all the eigenvalues are positive and so the branch is stable. If negative eigenvalues exist then their number is indicated by the number of negative signs on the branch – these branches are

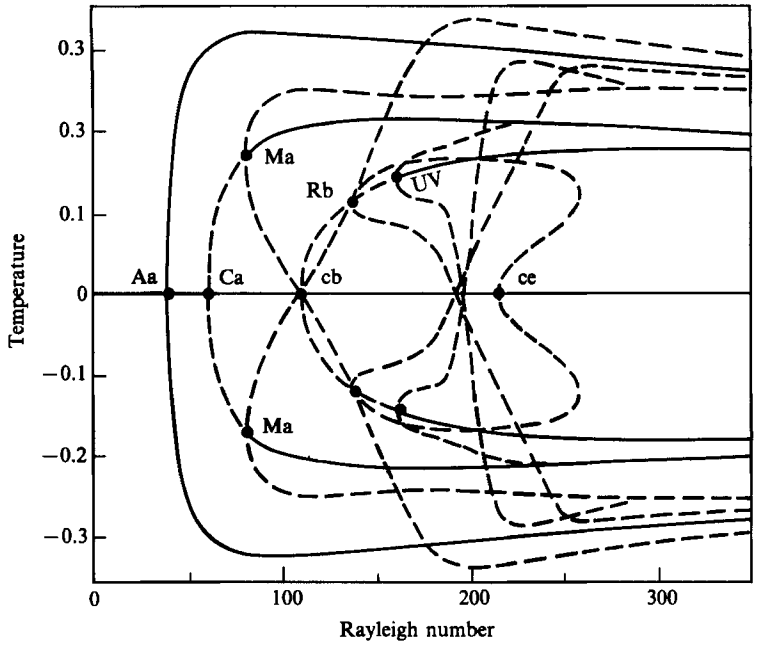

FIGURE 10. Computed bifurcation structure at $h = 1$ showing higher modes. Stable/unstable branches are denoted by full/broken curves respectively.

unstable. Aa and Ca denote the two primary bifurcation points and Ma the secondary bifurcation point.

The streamlines and isotherms are also displayed in figure 9 for the various modes when $Ra = 100$; these visualizations graphically confirm the statements concerning symmetry made in §3.3. We note that, as expected, the full solution set possesses the symmetries of the basic problem.

A rather fuller state diagram is given in figure 10 for Rayleigh numbers up to 350 and includes the primary bifurcations to the three-cell mode (3, 1) at cb. The three-cell solution branches have two secondary bifurcations at Rb and UV. These are necessary for the exchange of the primary (3, 1) mode with each of the two primary modes bifurcating at lower Rayleigh number. The bifurcation at Rb is subspace breaking and transcritical, whereas that at UV is centro-symmetry breaking and pitchfork. We note that the crossing at cb of the branches arising at the secondary bifurcations Ma is a consequence of the measure chosen; there are no bifurcations on these secondary branches at this point.

For clarity we have not shown in figure 10 the primary bifurcations located at Rayleigh number greater than 160, nor the secondary bifurcations associated with them, nor any tertiary bifurcations (we define a tertiary bifurcation to be a singular point on a branch that arises at a secondary bifurcation). Moreover, a primary bifurcation to a (2, 2) mode occurs at $Ra = 16\pi^2$ but the branch has zero measure and overlays the abscissa. A symmetry-breaking secondary bifurcation from this (2, 2) mode occurs at ce and the bifurcating branch connects with the secondary bifurcation at Rb on the (3, 1) branch.

To clarify this connectivity of the (3, 1) and (2, 2) solution branches, the schema of figure 11 represents the (2, 2) mode with non-zero measure. The supercritical branches arising at each of the transcritical points Rb on the (3, 1) primary branch

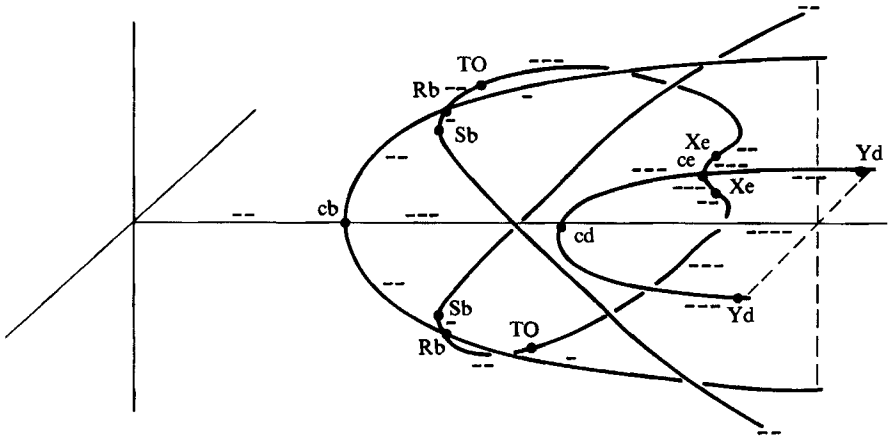

FIGURE 11. Schema of the detailed structure of the state diagram focusing on the (3, 1) and (2, 2) modes.

loop round to form a pitchfork bifurcation at ce on just *one* of the (2, 2) primary branches. This asymmetry is unexpected but is consistent with the nature of the (2, 2) primary bifurcation which is *not* $\mathbf{Z}_2 \times \mathbf{Z}_2$-symmetry breaking. We note that the bifurcation at ce is supercritical and the limit points between Rb and ce are a consequence of this. A further unexpected feature is the presence of centro-symmetry-breaking tertiary bifurcations at TO and Xe. These tertiary bifurcations are required for the modal exchange of secondary bifurcations. We further indicate on figure 11 two symmetrically disposed subcritical bifurcations at Yd on each of the (2, 2) branches.

With regard to figure 11, it is interesting to consider how the flow changes at various points along the branch arising at the subspace-breaking bifurcation from the (3, 1) mode, up to where the same branch emerges from the symmetry-breaking bifurcation from the (2, 2) mode. The streamlines and isotherms at various points along the branch are visualized in figure 12. By comparing II and III we see the effect of subspace breaking: the solution II is invariant under T_3^1 and T_3^2, the solution III is not, and both solutions are centro-symmetric. In progressing along the branch to IV the outer two cells increase in strength and break up the weaker middle cell into two; these two vortices then grow in strength to form the symmetrical (2, 2) mode seen at V. Thus the bifurcation at V breaks the reflection symmetries S_x and S_y, as it must do in order to preserve the centro-symmetry $S_x S_y$.

From the examples of isotherm distributions shown so far it is clear that the variation in the temperature gradient at the horizontal surface, and therefore in the local heat flux, depends strongly on the flow mode. It is interesting to enquire whether the average heat transfer for each mode is as disparate. We have computed the average Nusselt number defined by

$$\overline{Nu} = \int_{-\frac{1}{2}}^{\frac{1}{2}} \left.\frac{\partial \theta}{\partial y}\right|_{y=-\frac{1}{2}} \mathrm{d}x$$

along each of the branches shown in the state diagram of figure 10. The results are displayed in figure 13 and the significantly different heat transfer characteristics of the various stable modes are clearly apparent. This behaviour highlights most tellingly the practical need to establish the existence of multiple stable solutions and to assess the likelihood of stimulating each of them in particular circumstances.

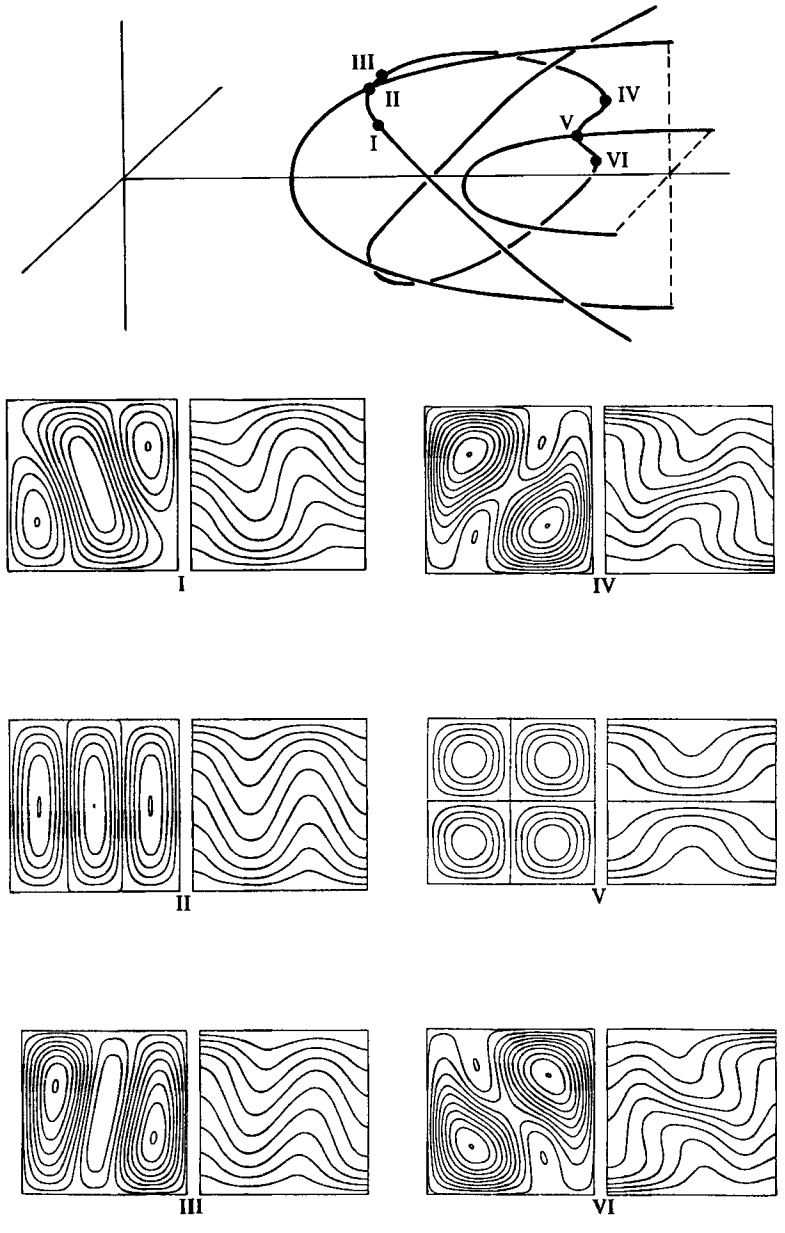

FIGURE 12. Flow development along the secondary branch connecting the (3, 1)- and (2, 2)-solution branches.

5.2. *The modal exchange processes*

The one- and two-cell flows exchange priority at $h = \sqrt{2}$; the development of the state diagrams as h increases through this critical value has been described in §3.2 and is not repeated here. The computed variation with h of the primary bifurcations to the (1, 1) and (2, 1) modes, in the neighbourhood of their intersection, is shown in figure 14 as curves AaB and CaD respectively. Secondary bifurcation off the two-cell branch occurs along Ma and off the one-cell branch along aN. It is interesting to note that figure 14 contains more information than is at first apparent. For as confirmed

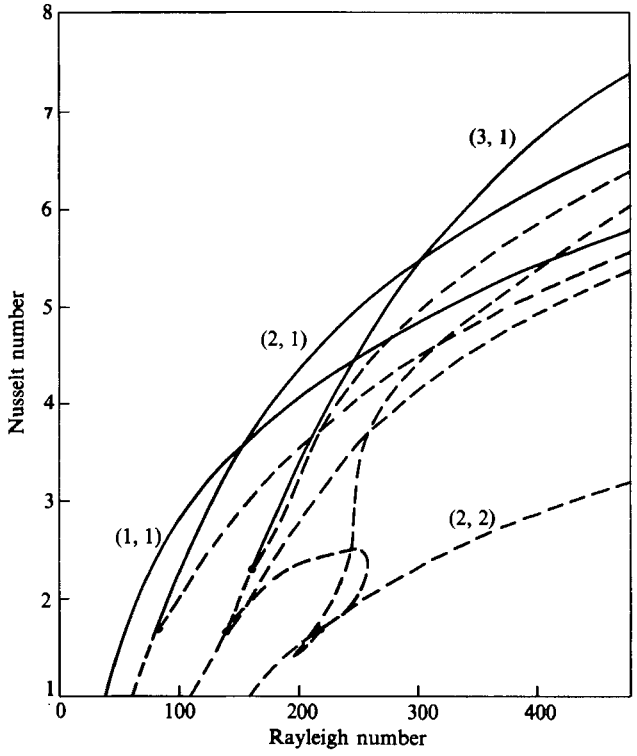

FIGURE 13. Variation of Nusselt number with Rayleigh number for the lower modes in a square cavity. Stable/unstable branches are denoted by full/broken curves respectively.

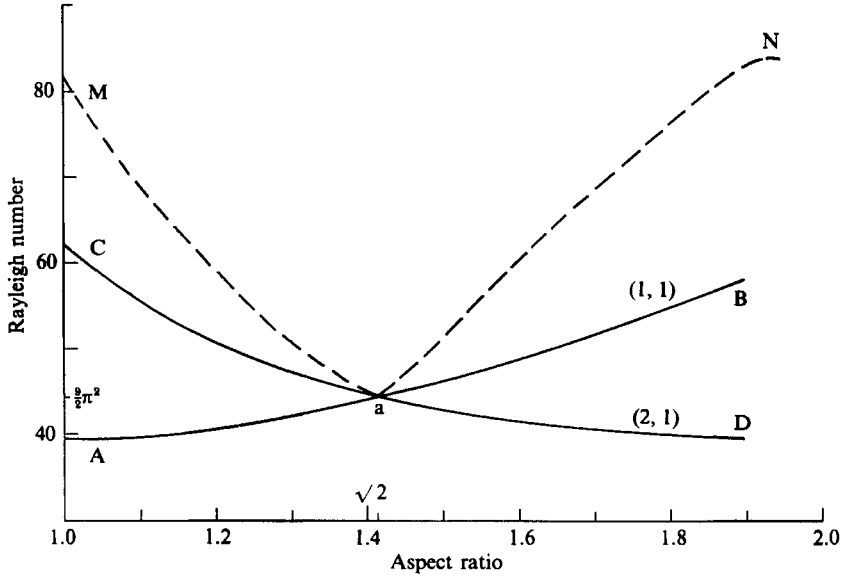

FIGURE 14. Computed variation with aspect ratio of the critical Rayleigh number for the primary bifurcations (full curves) and the secondary bifurcation (broken curves).

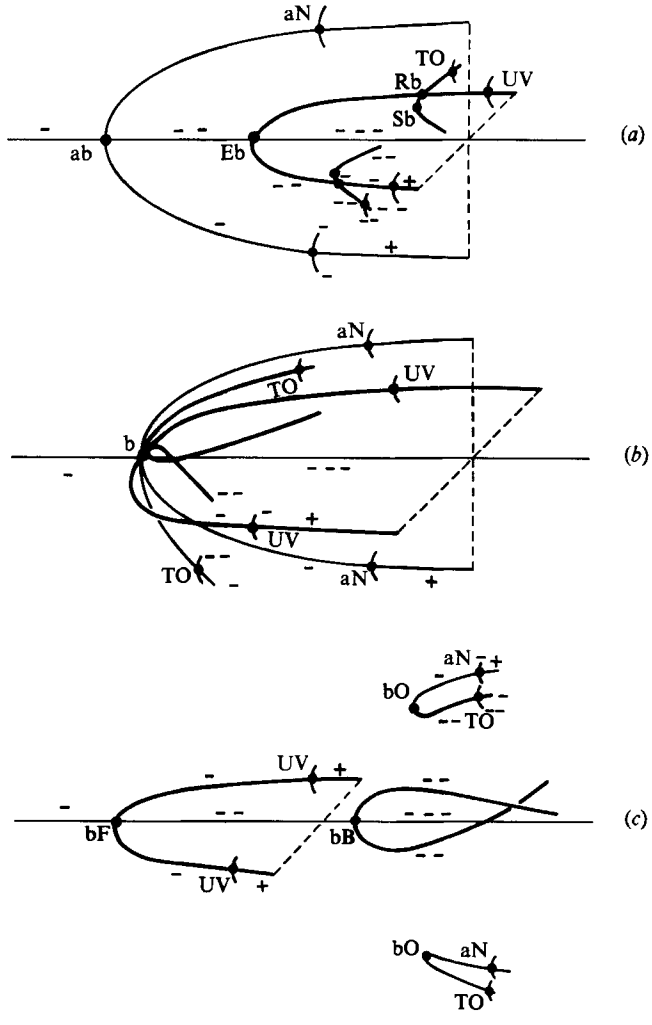

FIGURE 15. Schema of state diagrams for (1, 1)/(3, 1) interchange in the Lapwood problem. (*a*) $h < \sqrt{3}$, (*b*) $h = \sqrt{3}$, (*c*) $h > \sqrt{3}$.

by the weakly nonlinear analysis we know that the second primary mode is stabilized by the secondary bifurcation. Thus at fixed aspect ratio, the second primary (i.e. the one with the higher critical Rayleigh number) is stable for Rayleigh numbers larger than the Rayleigh number at which the secondary bifurcation occurs. In other words, both primary modes are stable for Rayleigh numbers above the curve MaN in figure 14, one of these modes at a given h being preferred and the other being anomalous as described in §5.1.

Consider now the one- and three-cell flows, which exchange priority at an aspect ratio of $\sqrt{3}$. The qualitative development of the state diagrams as h increases through this critical value is illustrated in figure 15. For $h < \sqrt{3}$ the unstable one-cell flows bifurcate from the trivial solution at ab, at a lower Rayleigh number than the unstable three-cell flows bifurcating at Eb, as sketched in 15(*a*). Both these bifurcations are supercritical, pitchfork, and they are associated with the breaking of reflectional symmetries S_x and S_y. Secondary bifurcation occurs at aN on the one-cell branch leaving it stable at higher Rayleigh number. The secondary bifurcations

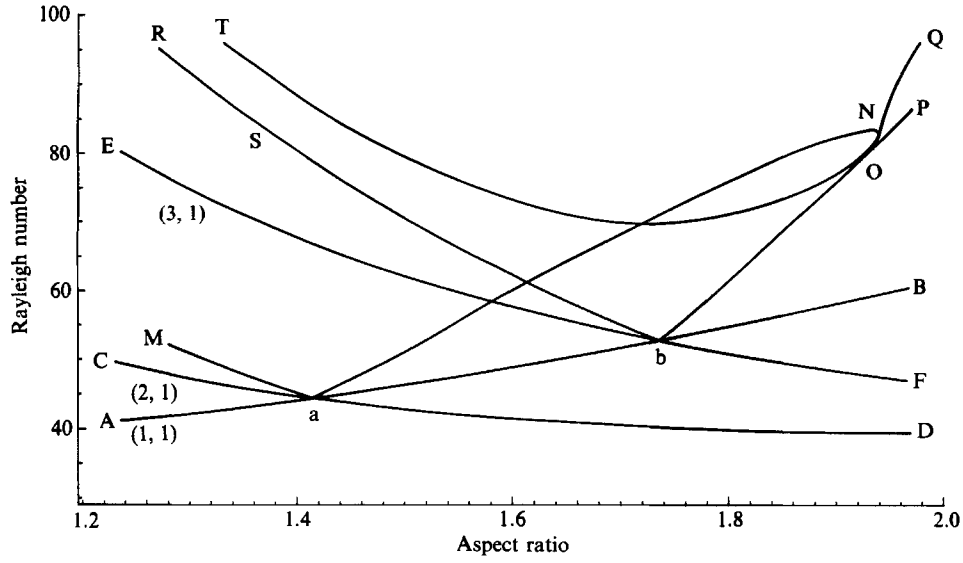

FIGURE 16. Computed loci of singular points near (1, 1)/(3, 1) neutral curve intersection in the Lapwood problem.

break the centro-symmetry $S_x S_y$ and are therefore pitchfork. In contrast the secondary bifurcations which occur on the three-cell branch at Rb are transcritical; the solutions on the bifurcating branches break out of the subspace which is invariant under the action of I, T_3^1 and T_3^2 but retain centro-symmetry as discussed in §5.1. These branches undergo further bifurcation at the tertiary points TO; these break the remaining centro-symmetry $S_x S_y$ and are therefore pitchfork. Finally, further secondary bifurcations on the three-cell branch at UV stabilize the three-cell flows at higher Rayleigh number. We note that for $\sqrt{2} < h < \sqrt{3}$ both the one- and three-cell stable flows are anomalous and the two-cell flows are preferred, the (2, 1) mode having the lowest critical Rayleigh number in this range.

As h approaches $\sqrt{3}$ the bifurcation points ab, Eb and Rb approach each other until they coincide at the modal exchange point b, as shown in figure 15(*b*). Concomitantly, the limit point Sb associated with the transcritical bifurcations approaches Rb so that the secondary bifurcation becomes pitchfork at the point of exchange. As h increases from $\sqrt{3}$, the multiple bifurcation structure of figure 15(*b*) unfolds to form the new structure sketched in figure 15(*c*). This unfolding creates new mixed-mode primary branches arising at the limit points bO. These mixed-mode branches are made up of branches which, for $h < \sqrt{3}$, corresponded to primary one-cell and secondary three-cell solutions. Along the mixed-mode branches there are secondary bifurcations at aN, which stabilize the primary flow for large Rayleigh numbers, and at TO, which was a tertiary bifurcation before the unfolding. The unfolding also creates new primary one-cell branches from those which, for $h < \sqrt{3}$, corresponded to secondary three-cell branches bifurcating from Rb through Sb (see figure 15*a*). The primary three-cell branches arising at Eb for $h < \sqrt{3}$ and bF for $h > \sqrt{3}$ lose the secondary bifurcation Rb during the exchange but are otherwise unaffected.

The schematic development of the state diagram of figure 15 was deduced from the computed variations with h of the primary and secondary bifurcation points which are presented in figure 16. The neutral stability curves for the primary one- and

three-cell branches are labelled abB and EbF respectively, and the modal exchange takes place at b. The lowest secondary bifurcation of the three-cell branch occurs along the path of transcritical points Rb. The associated path of limit points Sb lies very close to Rb and at the multiple bifurcation point b the transcritical and limit points coincide and the bifurcations become pitchfork. The other path of singular points involved in the modal exchange is labelled bOP and corresponds to the limit point on the disconnected branches drawn in figure 15(*c*). Clearly, as anticipated in §3.3, the exchange of the (1,1) and (3,1) modes is not described by the Schaeffer model. In fact, it is similar to and somewhat less complex than the interchange between two- and six-cell modes in the Taylor–Couette problem considered by Tavener & Cliffe (1988). In both cases the subspace breaking of the three-cell secondary bifurcation would seem to determine the special nature of the modal exchange. This subspace breaking is possible owing to the T_3^1 and T_3^2 translational invariance of the (3, 1) mode resulting from the slip conditions on the boundaries.

We have also included in figure 16 the (1, 1)/(2, 1) modal exchange that we have already discussed, because the path of one-cell secondary bifurcations aN which emerges from the point of exchange labelled a interacts unexpectedly with the path of limit points bOP emerging from the point of exchange b of the (1, 1) and (3, 1) modes. Specifically, the path of secondary bifurcation points aN turns back at N and becomes the path of bifurcation points NOT, with O being a point of osculation of the curves NOT and bOP. Further, a path of limit points NQ emerges from the path of bifurcation points aNO at N. This complex interaction takes place for aspect ratios $1.88 < h < 1.96$ and the paths of critical points in this range are shown in figure 17(*a*). This can be interpreted with reference to the development of the state diagrams for increasing h shown in figure 17(*b*). We first recall from figure 15 that as a result of the (3, 1)/(1, 1) exchange the secondary bifurcation aN lies, for $h > \sqrt{3}$, on one of the branches originating from the limit point bO – the secondary bifurcation TO lies on the other one. This is represented in the first state diagram of figure 17(*b*). As h increases, the point TO moves around the limit point bO and is then labelled ON, and this features on figure 17(*a*) near the osculation point of the path TON with bOP, i.e. at the double-singular point O. As h increases further the supercritical bifurcation ON develops quartic contact at point N (or very close to N; we have not attempted to numerically resolve the difference since the global stability map would not change). At N the bifurcations ON and aN coalesce and the two secondary branches disconnect in the opposite sense giving mixed-mode branches. The overall effect of this complex behaviour is to trace out a path aNOP above which a one-cell mode is stable. We note that the occurrence of a coalescence/quartic point N and double-singular point O in close proximity suggests that this structure results from the unfolding of a codimension-2 singularity as described by Jepson, Spence & Cliffe (1987).

An implication of the presence of the double-singular point is the possible generation of Hopf bifurcations. Although these do not necessarily arise at double singular points, figure 17(*b*) shows that they are expected in the present case in order to preserve the Leray–Schauder degree on the branches, for increasing h. The locating of such Hopf points is beyond the scope of the present study but for completeness we have included a conjectured path O? in figure 17(*a*) and we note two points: (*a*) we expect the Hopf bifurcations to stabilize a part of the branches on which they lie; (*b*) the Hopf bifurcations will have infinite period at O and so complex dynamical behaviour, possibly chaotic, may be expected in the neighbourhood of O.

We show in figure 18 the paths of all the singular points that we have computed.

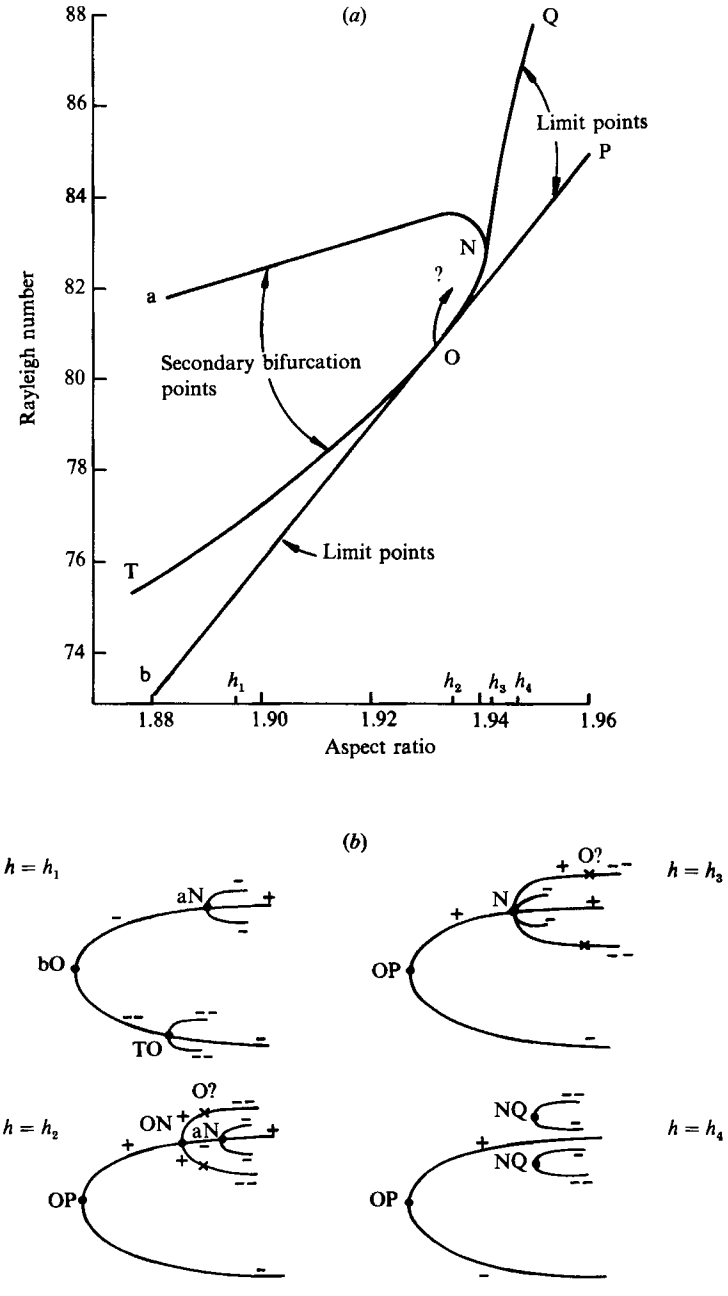

FIGURE 17. (*a*) The loci of the singular points on the disconnected mixed one-/three-cell branch with conjectured path of Hopf points. (*b*) The corresponding evolution of the state diagram as the aspect ratio increases.

In addition to the modal exchanges discussed so far, this figure includes five more, namely the exchange of the (2, 2) mode with the (3, 1), (4, 1) and (1, 2) modes, and the exchange of the (1, 2) mode with the (3, 1) and (4, 1) modes. We have not attempted to compute all the secondary bifurcations needed to elucidate the exchange mechanisms, except in the case of the (2, 2)/(3, 1) exchange which we describe below,

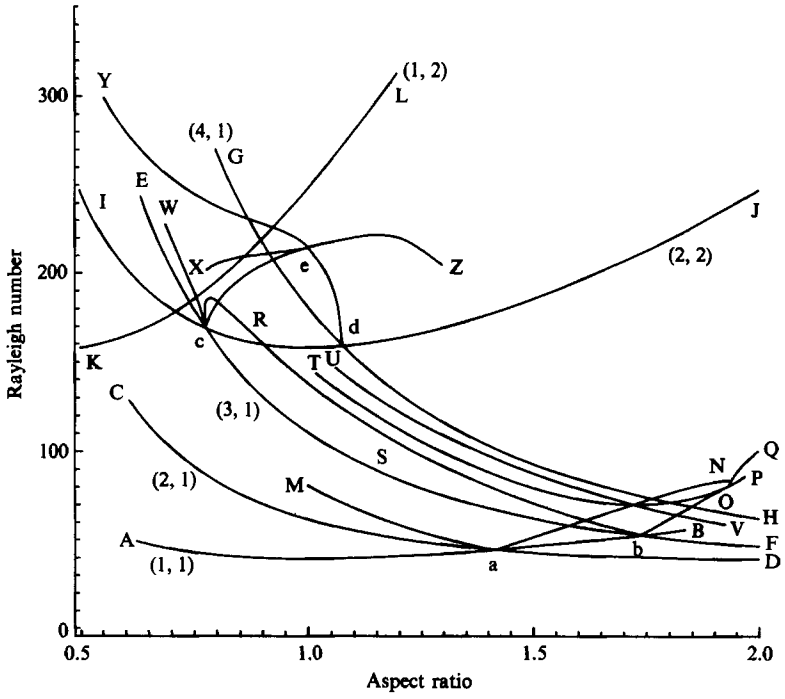

FIGURE 18. The full plot of computed loci of singular points.

and incompletely in the case of the (2, 2)/(4, 1) exchange where we see that the subcritical bifurcation Yd on the (2, 2) branch (see figure 11) originates at the point of exchange d. Figure 18 also includes the modal exchange of the secondary bifurcations cZ and Yd at e and we see that the tertiary bifurcation Xe appearing in figure 11 is involved in this exchange. In discussing the (3, 1)/(1, 1) exchanges we have seen how the nature of the symmetries preserved by the odd-cell solutions induces a special mechanism for the exchange which is different to the Schaeffer model. Similarly we expect that the (3, 1)/(2, 2) exchange will differ from the Schaeffer model and this is confirmed by the unusual linkage of these two modes at $h = 1$ illustrated in figure 11.

We show in figure 19(*a*) the computed paths of singular points in the neighbourhood of the exchange. Eb and Id are the paths of primary bifurcation points to the (3, 1) and (2, 2) modes respectively which intersect at *c*. Three paths of secondary bifurcations are involved in the exchange. For $h > (3/5)^{\frac{1}{2}}$ the (2, 2) mode undergoes secondary bifurcation on just one of its two branches along the line ce, as illustrated in figure 19(*b*). As h decreases through its critical value this single bifurcation passes onto the other branch emanating from the primary (2, 2) bifurcation to trace out the path Wc. The transcritical secondary bifurcations on the (3, 1) branches trace out the path cR and become pitchfork at c where they coincide. From figure 19(*b*) we see that the effect of this exchange is to 'unravel' for $h < (3/5)^{\frac{1}{2}}$ the linkage found for $h > (3/5)^{\frac{1}{2}}$.

We turn finally to the practical import of the results we have presented. In figure 18 we showed a complete picture of the paths of computed singular points in (Ra, h) parameter space. Most of those paths are unphysical in the sense that they represent bifurcations on an unstable branch which leave the branch unstable. The physically important paths, fewer in number, are those that stabilize branches and

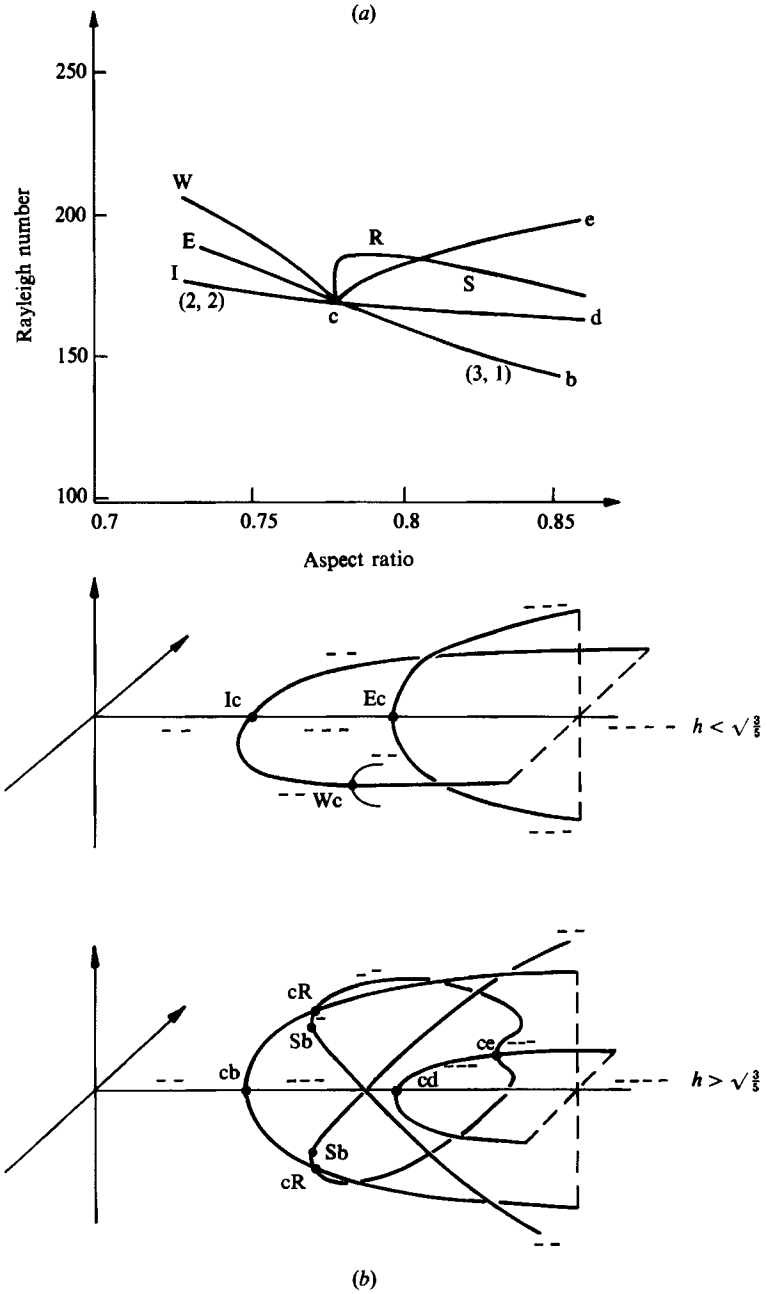

FIGURE 19. (*a*) The computed loci of singular points near (2, 2)/(3, 1) neutral curve intersection. (*b*) Schema showing the evolution of the state diagram as the aspect ratio increases.

it might appear that these are the only ones with which we should be concerned. However, an important conclusion of our study is that the behaviour of the 'physical' bifurcations is intimately connected with that of the 'unphysical' ones, and that a complete understanding can be arrived at only by considering them all. As an illustration of this point, we show in figure 20 the domain of existence of the various alternative stable flows in (Ra, h)-space, obtained by suppressing the paths

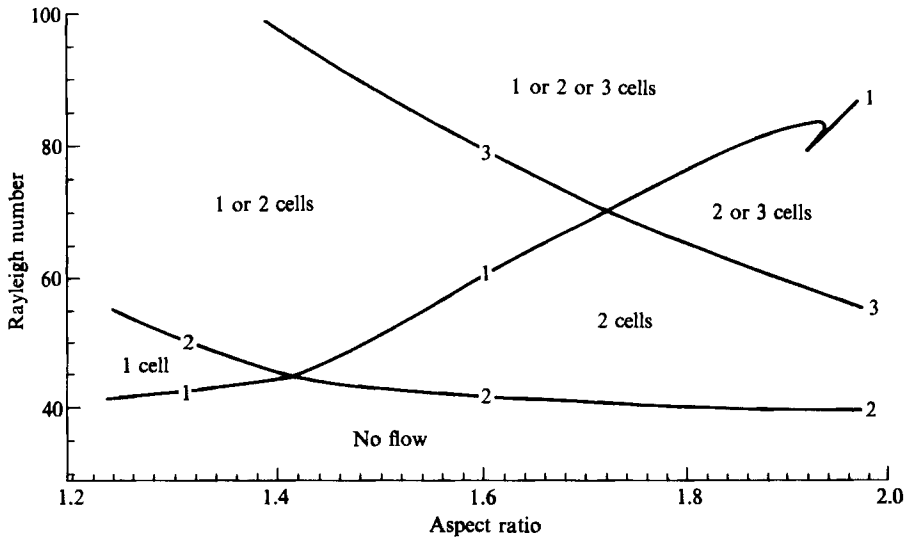

FIGURE 20. Stability map showing the domains of the alternative physical flows.

of 'unphysical' bifurcations. This clearly shows the complicated shape of the stability boundary for one-cell flows and we recall that this results from the complex interactions between paths of singular points, both physical and unphysical, described in figure 16.

6. Conclusions

Analytical and numerical techniques were used to study Lapwood convection in a two-dimensional saturated porous cavity. For a cavity of fixed aspect ratio, a simple analytical linear stability study shows that a countably infinite set of eigenmodes exists. These eigenmodes occur at discrete eigenvalues and represent convective flows with m and n rolls in the horizontal and vertical directions, respectively. The preferred mode of convection (the one with the lowest critical Rayleigh number) always has one cell in the vertical direction: the number of cells in the horizontal direction depends upon the aspect ratio.

A comprehensive state diagram for a cavity of unit aspect ratio was computed and shown to have an unexpectedly complex structure. For low enough Rayleigh number, the preferred mode is always stable, the domain of stability being limited by the occurrence of Hopf bifurcations at higher Rayleigh numbers. Secondary bifurcations stabilize other primary solution branches and give rise to the possibility of anomalous modes of convection. The flow and temperature fields associated with the solution branches were visualized.

As the aspect ratio increases, modal exchanges take place in which secondary and even tertiary bifurcations play a necessary rôle. By using a synthesis of degree theory, symmetry arguments and continuation methods, the exchange processes were elucidated. Detailed results were obtained for the $(1,1)/(2,1)$ and $(1,1)/(3,1)$ exchanges and a stability map for these three modes was determined for aspect ratios between 1 and 2. This stability map shows the domains of the alternative physical flows and illustrates most clearly their non-unique nature.

The study also revealed a complex asymmetrical connectivity between the $(3,1)$

and (2, 2) modes; this feature is believed to arise because of the underlying symmetries of the modes and is being studied further. Although the (2, 2) mode is unphysical in the sense that it is always unstable, it is the (2, 2)/(3, 1) exchange which gives rise to a secondary bifurcation that stabilizes a one-cell branch. This illustrates well the need to study bifurcations to both stable and unstable flows, in order to determine stability boundaries.

In summary, the results of this study of Lapwood convection provide important information on: how anomalous patterns form; how many anomalous patterns are expected for given operating conditions; how the heat transfer depends on the anomalous patterns; how the preferred and anomalous modes change with varying container size.

It is a pleasure to thank K. A. Cliffe for helpful discussions and for allowing us to quote his work with S. Tavener. The work described in this report is part of the longer term research carried out within the Underlying Programme of the United Kingdom Atomic Energy Authority. D.S.R. wishes to thank the SERC for partial support towards the costs of this research programme.

REFERENCES

AIDUN, C. K. & STEEN, P. H. 1987 Transition to oscillatory convective heat transfer in fluid-saturated porous medium. *J. Thermophys.* **1**, 268.

BAUER, L., KELLER, H. B. & REISS, E. L. 1975 Multiple eigenvalues lead to secondary bifurcation. *SIAM Rev.* **17**, 101.

BECK, J. L. 1972 Convection in a box of porous material saturated with fluid. *Phys. Fluids* **15**, 1377.

BORIES, S. A. 1985 Natural convection in porous media. *Proc. NATO ASI on Fundamentals of Transport Phenomena in Porous Media.*

BORIES, S. A., COMBARNOUS, M. A. & JAFFRENNOU, J. Y. 1972 Observation des différentes formes d'écoulements convectifs dans une couche poreuse inclinée. *C.R. Acad. Sci. Paris* A **275**, 857.

BORKOWSKA-PAWLAK, B. & KORDYLEWSKI, W. 1982 Stability of two-dimensional natural convection in a porous layer. *Q. J. Mech. Appl. Maths*, **35**, 279.

BORKOWSKA-PAWLAK, B. & KORDYLEWSKI, W. 1985 Cell-pattern sensitivity to box configuration in a saturated porous media. *J. Fluid Mech.* **150**, 169.

CALTAGIRONE, J. P. 1975 Thermoconvective instabilities in a horizontal porous layer. *J. Fluid Mech.* **72**, 269.

CALTAGIRONE, J. P., CLOUPEAU, M. & COMBARNOUS, M. A. 1971 Convection naturelle fluctuante dans une couche poreuse horizontale. *C. R. Acad. Sci. Paris* B **273**, 833.

CALTAGIRONE, J. P., MEYER, G. & MOJTABI, A. 1981 Structurations thermoconvectives tridimensionelles dans une couche poreuse horizontale. *J. Méc.* **20**, 219.

CLIFFE, K. A. 1983 Numerical calculations of two-cell and single-cell Taylor flows. *J. Fluid Mech.* **135**, 219.

CLIFFE, K. A. 1988 Numerical calculations of the primary flow exchange process in the Taylor Problem. *J. Fluid Mech.* **197**, 57.

CLIFFE, K. A. & WINTERS, K. H. 1984 A numerical study of the cusp catastrophe for Bénard convection in tilted cavities. *J. Comp. Phys.* **54**, 531.

CLIFFE, K. A. & WINTERS, K. H. 1986 The use of symmetry in bifurcation calculations and its application to the Bénard problem. *J. Comp. Phys.* **67**, 310.

COMBARNOUS, M. A. & LEFUR, B. 1969 Transfert de chaleur par convection naturelle dans une couche poreuse horizontale. *C. R. Acad. Sci. Paris* B **269**, 1009.

GOLUBITSKY, M. & SCHAEFFER, D. G. 1985 *Singularities and Groups in Bifurcation Theory*, Part I. Springer.

HOLST, P. H. & AZIZ, K. 1972 Transient three-dimensional natural convection in confined porous media. *Intl J. Heat Mass Transfer* **15**, 73.

HORNE, R. N. 1979 Three-dimensional natural convection in a confined porous medium heated from below. *J. Fluid Mech.* **92**, 751.

HORNE, R. N. & O'SULLIVAN, M. J. 1974 Oscillatory convection in a porous medium heated from below. *J. Fluid Mech.* **66**, 339.

JACKSON, C. P. 1987 A finite-element study of the onset of vortex shedding in flow past variously shaped bodies. *J. Fluid Mech.* **182**, 23.

JACKSON, C. P. & WINTERS, K. H. 1984 A finite-element study of the Bénard problem using parameter-stepping and bifurcation search. *Intl J. Num. Meth. Fluids* **4**, 127.

JEPSON, A. D. & SPENCE, A. 1984 Singular points and their computation. In *Numerical Methods for Bifurcation Problems* (ed. T. Küpper, H. D. Mittleman & H. Weber). International Series of Numerical Mathematics, Vol. 70. Birkäuser.

JEPSON, A. D., SPENCE, A. & CLIFFE, K. A. 1987 The numerical solution of nonlinear equations having several parameters. Part III: equations with $\mathbf{Z}_2$-symmetry. *Harwell Rep.* TP.1210, and submitted to *SIAM J. Num. Anal.*

KELLER, H. B. 1977 Numerical solutions of bifurcation and nonlinear eigenvalue problems. In *Applications of Bifurcation Theory* (ed. P. H. Rabinowitz), pp. 359–384. Academic.

KIDACHI, H. 1982 Side wall effect on the pattern formation of the Rayleigh–Bénard convection. *Prog. Theor. Phys.* **68**, 49.

KIMURA, S., SCHUBERT, G. & STRAUS, J. M. 1987 Instabilities of steady, periodic, and quasi-periodic modes of convection in porous media. *Trans. ASME* C: *J. Heat Transfer* **109**, 350.

METZENER, P. 1986 The effect of rigid sidewalls on nonlinear two-dimensional Bénard convection. *Phys. Fluids* **29**, 1373.

MOORE, G. & SPENCE, A. 1980 The calculation of limit points of non-linear equations. *SIAM J. Numer. Anal.* **17**, 567.

REES, D. A. S. & RILEY, D. S. 1986 Free convection in an undulating saturated porous layer: resonant wavelength excitation. *J. Fluid Mech.* **166**, 503.

REES, D. A. S. & RILEY, D. S. 1989*a* The effects of boundary imperfections on convection in a saturated porous layer: near-resonant wavelength excitation. *J. Fluid Mech.* **199**, 133.

REES, D. A. S. and RILEY, D. S. 1989*b* The effects of boundary imperfections on convection in a saturated porous layer: non-resonant wavelength excitation. *Phil. Trans. R. Soc. Lond.* (Submitted.)

RILEY, D. S. & WINTERS, K. H. 1986 The onset of convection in a porous medium: a preliminary study. *Harwell Rep.* R.12586.

RILEY, D. S. & WINTERS, K. H. 1987 A bifurcation study of convection in a two-dimensional saturated porous cavity. *Harwell Rep.* TP.1246 and *Bifurcation Phenomena in Thermal Processes and Convection*, *HTD*, Vol. 94 and *AMD*, Vol. 89. ASME.

SCHAEFFER, D. G. 1980 Qualitative analysis of a model for boundary effects in the Taylor problem. *Proc. Camb. Phil. Soc.* **87**, 307.

SHEARER, M. 1980 Secondary bifurcation near a double eigenvalue *SIAM J. Math. Anal.* **11**, 365.

STEEN, P. 1983 Pattern selection for finite-amplitude convection states in boxes of porous media. *J. Fluid Mech.* **136**, 219.

STEEN, P. 1985 Container geometry and the transition to unsteady Bénard convection in porous media. *Phys. Fluids* **29**, 925.

SCHUBERT, G. & STRAUS, J. M. 1979 Three-dimensional and multi-cellular steady and unsteady convection in fluid-saturated porous media at high Rayleigh numbers. *J. Fluid Mech.* **94**, 25.

STRAUS, J. M. 1974 Large amplitude convection in porous media. *J. Fluid Mech.* **64**, 51.

STRAUS, J. M. & SCHUBERT, G. 1978 On the existence of three-dimensional convection in a rectangular box containing fluid-saturated porous material. *J. Fluid Mech.* **87**, 385.

STRAUS, J. M. & SCHUBERT, G. 1979 Three-dimensional convection in a cubic box of fluid-saturated porous material. *J. Fluid Mech.* **91**, 155.

STRAUS, J. M. & SCHUBERT, G. 1981 Modes of finite-amplitude three-dimensional convection in rectangular boxes of fluid-saturated porous material. *J. Fluid Mech.* **103**, 23.

SUTTON, F. 1970 Onset of convection in a porous channel with net through flow. *Phys. Fluids* **13**, 1931.

TAVENER, S. & CLIFFE, K. A. 1988 Primary flow exchange mechanisms in Taylor–Couette flow applying non-flux boundary conditions. *Harwell Rep.* TP.1316.

WERNER, B. 1984 Regular systems for bifurcation points with underlying symmetries. In *Numerical Methods for Bifurcation Problems* (ed. T. Küpper, H. D. Mittleman & H. Weber). International Series of Numerical Mathematics, Vol. 70. Birkhäuser.

WINTERS, K. H. 1987*a* Hopf bifurcation in the double-glazing problem. *Harwell Rep.* TP.1187, and *Trans. ASME* C: *J. Heat Transfer* **109**, 894–898.

WINTERS, K. H. 1987*b* A bifurcation study of laminar flow in a curved tube of rectangular cross-section. *J. Fluid Mech.* **180**, 343.

WINTERS, K. H. 1987*c* Oscillatory convection in crystal melts: the horizontal Bridgman process. In *Proc. 5th Intl Conf on Numerical Methods in Thermal Problems, Montreal*, pp. 299–310. Swansea: Pineridge.

WINTERS, K. H. & BRINDLEY, R. C. G. 1984 Multiple solutions for laminar flow in helically-coiled tubes. *Harwell Rep.* R.11373.

WINTERS, K. H. & BROWN, T. W. 1985 Bénard convection in a three-dimensional cavity: the effects of aspect ratio and tilt. In *Proc. 4th Intl Conf. on Numerical Methods in Thermal Problems, Swansea*, pp. 376–385. Swansea: Pineridge.

WINTERS, K. H. & CLIFFE, K. A. 1985 The prediction of critical points for thermal explosions in a finite volume. *Combust. Flame* **62**, 13.

WINTERS, K. H., CLIFFE, K. A. & JACKSON, C. P. 1984 A review of extended systems for finding critical points in coupled problems. In *Proc. Conf. on Numerical Methods for Transient and Coupled Problems* (ed. R. W. Lewis, E. Hinton, P. Bettess & B. A. Schrefler), pp. 949–959. Swansea: Pineridge.

WINTERS, K. H., CLIFFE, K. A. & JACKSON, C. P. 1987 The prediction of instabilities using bifurcation theory. *Numerical Methods for Transient and Coupled Problems* (ed. R. W. Lewis, E. Hinton, P. Bettess & B. A. Schrefler), pp. 179–198. Wiley.

WINERS, K. H., PLESSER, TH. & CLIFFE, K. A. 1988 The onset of convection in a finite container due to surface tension and buoyancy. *Physica* **29D**, 387–401.